HYGROTHERMAL FRACTURE ANALYSIS OF FIBROUS COMPOSITES WITH VARIABLE FIBER SPACING USING JK-INTEGRAL

A THESIS SUBMITTED TO
THE GRADUATE SCHOOL OF NATURAL AND APPLIED SCIENCES
OF
MIDDLE EAST TECHNICAL UNIVERSITY

BY

FARID SAEIDI

IN PARTIAL FULFILLMENT OF THE REQUIREMENTS
FOR
THE DEGREE OF MASTER OF SCIENCE
IN
MECHANICAL ENGINEERING

JANUARY 2013

HYGROTHERMAL FRACTURE ANALYSIS OF FIBROUS COMPOSITES WITH VARIABLE FIBER SPACING USING JK-INTEGRAL

Submitted by **FARID SAEIDI** in partial fulfillment of the requirements for the degree of **Master of Science in Mechanical Engineering, Middle East Technical University** by,

Prof. Dr. Canan ÖZGEN _____
Dean, Graduate School of **Natural and Applied Sciences**

Prof. Dr. Suha Oral _____
Head of Department, **Mechanical Engineering**

Assoc. Prof. Dr. Serkan DAĞ _____
Supervisor, **Mechanical Engineering Dept., METU**

Examining Committee Members:

Prof. Dr. Suat KADIOĞLU _____
Mechanical Engineering Dept., METU

Assoc. Prof. Dr. Serkan DAĞ _____
Mechanical Engineering Dept., METU

Prof. Dr. Bora YILDIRIM _____
Mechanical Engineering Dept., HU

Asst. Prof. Dr. Yiğit YAZICIOĞLU _____
Mechanical Engineering Dept., METU

Asst. Prof. Dr. Gökhan ÖZGEN _____
Mechanical Engineering Dept., METU

Date: 1/24/2013

I hereby declare that all information in this document has been obtained and presented in accordance with academic rules and ethical conduct. I also declare that, as required by these rules and conduct, I have fully cited and referenced all material and results that are not original to this work.

Name, Last name: Farid SAEIDI

Signature:

ABSTRACT

HYGROTHERMAL FRACTURE ANALYSIS OF FIBROUS COMPOSITES WITH VARIABLE FIBER SPACING USING JK-INTEGRAL

SAEIDI, Farid
M.Sc., Department of Mechanical Engineering
Supervisor: Assoc. Prof. Dr. Serkan DAĞ

January 2013, 68 pages

In this study, a J_k-integral based computational method will be developed to conduct fracture analysis of fibrous composite laminates that possess variable fiber spacing. This study will be carried out for the fibrous composites exposed to not only thermal but also hygroscopic boundary condition, which results hygrothermal load. Formulation of the J_k-integral will be carried out by using the constitutive relations of plane orthotropic hygrothermoelasticity. One of the most important challenges of this study is to change J_k-integral formulation into domain independent form, because dealing with infinitely small domains in solving the integral would be frustrating. Developed form of J_k-integral will be merged to ANSYS, a finite element analysis software. Numerical results will be generated so as to assess the influence of variable fiber spacing on the modes I and II stress intensity factors, energy release rate, and the T-stress.

For validation and comparison, some of the results are also obtained using Displacement Correlation Technique (DCT).

Keywords: J_k-integral, Variable Fiber Spacing, Hygrothermoelasticity, T-stress, Finite Element Method, Fibrous Composite.

ÖZ

DEĞİŞKEN ELYAF ARALIĞINA SAHİP ELYAF TAKVİYELİ KOMPOZİTLERİN JK-İNTEGRALİ İLE HİGROTERMAL KIRILMA ANALİZİ

SAEIDI, Farid
Yüksek Lisans, Makina Mühendisliği Bölümü
Tez Yöneticisi: Doç. Dr Serkan DAĞ

Ocak 2013, 68 sayfa

Bu çalışmada, bir J_k-integral bazlı hesaplama yöntemi, değişken fiber aralığına sahip lifli kompozit laminatlarda kırılma analizi yapmak için geliştirilecektir. Bu çalışma sadece termal yükü degil,hem de higroskopik sınır koşuluna maruz elyaf kompozitler için yapılacaktır. J_k-integral formülasyonu düzlemi ortotropik hygrothermoelasticity ve bünye bağıntıları kullanılarak yapılacaktır. Çözmede sonsuz küçük alanlar'ile çalışmak zor olduğu için, formülasionu alan bağımsız hale getirmek buçalışmanin en önemli uğraşlarından birisidir. Alanbağımsız hale geliştirilen J_k-integral genel amaçlı sonlu elemanlar analiz program ANSYS'e entegre edilecektir. Elyaf aralığının mod I ve II gerilme şiddeti çarpanları, enerji bırakma miktarı ve T-gerilmesi üzerinde ki etkileri ni araştırmak için parametrick analizler yapılacaktır.

Doğrulama ve karşılaştırma için, bazı sonuçlar Hacmi Korelasyon Tekniği (DCT) kullanılarak elde edilmiştir.

Anahtar Kelimeler: J_k-integral, Değişken Fiber Aralığı, Hygrothermoelasticity, T-gerilmesi, Sonlu ElemanlarYöntemi, Lifli Kompozit.

To My Family

ACKNOWLEDGMENTS

I would like to express my gratitude to my supervisor Assoc. Prof. Dr. Serkan DAĞ without, whose knowledge and assistance this study would not have been successful, and I would like to thank him for his help and guidance and support during this study.

I would like to thank my Parents for their endless love, support and encouragement despite all hardship during this period.

I would like to thank my sister and also a future member of our family and my lifetime friend who gave me all the emotion and motivation needed to pass this challenging period of my life.

TABLE OF CONTENTS

LIST OF TABLES

TABLES

LIST OF FIGURES

FIGURES

LIST OF SYMBOLS

a.....Half crack length
h.....Total thickness of composite medium
h_1.....Thickness of the medium below crack
V_{f_0}.....Minimum fiber volume in the medium
V_{f_w}.....Maximum fiber volume in the medium
P.....Exponent defining the properties of the sheet
T_0.....Initial reference temperature
c_0.....Initial reference moisture concentration
V_f.....Fiber volume
V_m.....Matrix volume
W.....Mechanical strain energy density function
W^+.....Mechanical strain energy density function at the upper crack face
W^-.....Mechanical strain energy density function at the lower crack face
J_k.....J_k-integral
q.....q function
z_k.....Complex variable
x_k.....Real part of complex variable
y_k.....Imaginary part of complex variable
μ_k.....Roots of characteristic equation
α_k.....Real part of roots of characteristic equation
β_k.....Imaginary part of roots of characteristic equation
a_{ij}.....Compliance coefficient
E_i.....Modulus of elasticity
G_i.....Shear modulus if elasticity
K_I.....Mode I stress intensity factor
K_{II}.....Mode II stress intensity factor
x_1.....Global coordination principal axe x
x_2.....Global coordination principal axe y
T_s.....T-stress
R.....Radius of integration domain
d_k.....Length of lines used for approximation of $(W^+ - W^-)$
Γ_ε.....The curve over which J_k-integral is defined
A.....Domain integral area
Γ_{cr}.....Closed curve surrounding the area A
σ_{ij}.....Stress tensor
ε_{ij}.....Strain tensor
n_i.....Unit vector normal to the integration path
u_i.....Displacement components
δ.....Kronecker's delta
v_{ij}.....Poisson's ratios
α_i.....Thermal expansion coefficients
β_i.....Moisture expansion coefficients
ΔT.....Temperature difference
Δc.....Moisture concentration difference

CHAPTER 1

INTRODUCTION

1.1. Objective of the Study

The main goal of this study is to find a new extension of J_k - integral formulation and utilize it as a computational method for calculation of fracture parameters, for fibrous composites with variable fiber spacing subjected to hygrothermal stresses. Constitutive relations of plane orthotropic hygrothermoelasticity were used in developing the J_k - integral formulation for hygrothermal loading; and then shifted to a formulation of line and area integrals with independency from domain of integration.

Determining fracture parameters of the crack in the model involved several steps during the analysis. Initially, modeling the composite medium and in the second step discretizing the model for using finite element method. Third step was defining mechanical properties, boundary conditions and constraints of the composite sheet. In the fourth step, solution was carried out using a commercial program and these results were changed to structural loads to obtain stress field, strain and displacement in the plate. The last step in the solution was developing a code to use a numerical method to use results of the analysis to obtain numerical solution for the integral which gives out desired fracture parameters of the medium.

Finite element method was used for implementation of new form of J_k-integral. Process of the algorithm designed to obtain hygrothermal fracture parameters solution, is carried out using a general purpose finite element program ANSYS [37]. The computation of fracture parameters in the fibrous composite sheet with variable spaced fiber, involved modeling of an embedded crack in sheet, which is presumed to be in plane stress state and steady state boundary conditions. J_k-integral is used as a numerical method to solve the governing partial equations of hygroscopic and thermal fields. Some results are presented in order to validate the independency of the J_k-integral method from integration domain, also T-stress and energy release rate is presented as additional crack parameters. Numerical solutions are generated for cracks located in various locations of the composite sheet, also effect of minimum fiber density in the composite sheet, which is changing the function of fiber distribution in the whole sheet is investigate through the same solution for individual models.

1.2. Literature Survey

Fracture analysis of engineering structures is processed using different computational methods. J_k-integral is the most useful method, because stress intensity factors (SIFs), T-stress, and also energy release rate can be calculated, however in calculations based on other methods, obtaining all three factors at the same time is not possible. J_k-integral is equal to J_1-integral when k=1 and having another component when k=2, it's defined as a vector at crack tip [11-12]. J_k-integral calculation in this study is carried out by developing a domain independent form of the formulation at crack tip, in terms of line and area integrals.

Knowles and Sternberg [13] used J_k-integral to prove that a definite conservation law which is a part of this formulation on a definite line and three other similar conservation laws can be generated using principle of stationary potential energy and principles of invariant variational. Hellen and Blackburn [14] also used J_k-integral to find stress intensity factors for elastic materials to probe the direction of

maximum energy release rate and used it for comparison with experimental outcomes. In this study it's shown that plastic effects are getting more significant at the time when shear stress is the dominant stress, so for this case calculations would have good accuracy. Known as one of the first implementers of J_k-integral in fracture, Budiansky and Rice [15] related path independent Jk-integral to energy release rate associated with cavity or crack rotation, and expansion rate. Four different formulations of J_k-Integral were developed for multifarious engineering materials as a solution for the fracture problems of materials with specific properties. Chen and Ting [16, 17] used this formulation in conjunction with finite element method to calculate mixed-mode fracture parameters of crack with thermal boundary condition. Chang and Wu [18] developed a numerical calculation procedure for fracture analysis of curved cracks embedded in anisotropic elastic materials. Similar to other efforts dealing with path independency and singularity at the crack tip are one of the challenges in their study. Chu and Hong [19], also used the $J_k$integral independent of the integration path to calculate mixed-mode SIFs in anisotropic plates.

Pan and Amadei [20] have used BEM method to solve J_k-integral in 2D anisotropic materials, whereas Sollero and Aliabadi [21] used the same technique to carry out a fracture analysis on anisotropic materials. The difference between two techniques of two previous studies is the process of solving the integral and gathering displacements and tractions need for calculation; functionally graded materials under mechanical or thermal stresses. Khandelwal and Kishen [22-23] developed and fracture analysis procedure for biomaterials and found that J_k-integral gives accurate SIF results for crack embedded between two distinct materials. Technical literature survey shows that, J_k-integral have never been implemented before to be used as a technique for fracture analysis of advanced composites and engineering materials subjected to hygrothermal loading. Dag, Arman, and Yildirim [24], studied fracture parameters of orthotropic FGMs subjected to steady state and transient thermal loads by using finite element method and J_k-integral. Periodic cracks As a Distinct case of crack was also modeled and analyzed. In another study prior to [24] Dag and Yildirim [25], computationally solved J_k-integral for inclined cracks in the FGMs using finite element method to find parameters related to fracture analysis of the medium. Actually Dag [26], for the first time used $J_k$integral method to in order to find fracture parameters of FGMs under thermal loading. This study was carried out using finite element method to analyze periodic cracks and thermal shock heating in addition to normal crack and steady-state thermal load. Kim and Paulino [28] used $J_k$integral, Displacement Correlation Technique and crack closure integral as three different techniques to calculate stress intensity factors in FGMs. Outcome of these methods were compared with experimental results. Later Kim and Paulino [29] used J_k-integral for fracture analysis of nonhomogeneous materials having orthotropy with either changing or linear material properties for cracks having arbitrary orientation. Eischen [30] solved J_2-integral using a new technique to increase efficiency of this integral in calculation of J_k-integral.

According to the literature survey little efforts were made in the field of fracture analysis of hygrotheramally loaded materials, some of them are as presented as follows: Dag et al. [31] solved J_k-integral by the means of finite element method, to find fracture parameters of an orthotropic model under hygrothermal boundary condition. The material was FRC having equally spaced unidirectional fibers which made such a composite laminate orthotropic. Lee and Lee [32] carried out the fracture analysis of an IC plastic package under hygrothermal boundary condition using J-integral and finite difference method. In this study the possibility of delamination during definite soldering process called infrared heating was investigated. Ergun, Tasgetiren and Topcu [33] used experimental and numerical techniques to find first mode intensity factor and fatigue life in the aluminum patched with composite plates exposed to hygrothermal boundary condition.

1.3. Fiber reinforced Composites with Variable Fiber Spacing

Most of the engineering materials are sensitive to temperature and moisture concentration in the environment, causing deformation in the material. Among these materials polymer matrix Fiber reinforced composites are the ones used widely in industry and it is critically important to analyze their behavior when subjected to temperature and moisture concentration. Composite plates are made of several layers called laminas, and traditionally in Fiber reinforced laminas fibers are parallel and

uniformly spaced. However, disturbing isotropy of the laminas by controlling space between fibers to gain more stiffness, where the fibers are laid close to each other, and less density at the regions that fibers have more distance from each other, more efficient laminas than traditional ones can be fabricated [1], so by taking the loads and boundary conditions of the lamina into consideration and changing the fiber content in definite locations in the plate, relatively higher performances can be achieved. In this study behavior of a middle crack embedded in this special type of fibrous composite subjected to the hygrotheramal boundary conditions was investigated using J_k-integral. Utilizing composite plates with variable fiber spacing is increasing every day in industry, as a result scientific efforts are relatively increasing in this field. Some of these efforts are, manipulating Hedgepeths Shear-lag analysis to find stress concentration factors in a numerically simulated composite, with randomly and unidirectionally spaced fibers [2], investigation of sensitivity of the strength of metal-matrix composites with non-uniform and uniform fiber spacing to yield stress and stress distribution in them and also probing the effects of non-uniformity and breakage of fibers in stress distribution and tensile strength [3, 4]. Solution of plane stress problem for composite sheets with variable fiber spacing was obtained, using Ritz method as an approximation method for comparison with exact solution by Leissa and Martin [5]. Leissa and Martin [6] also using Ritz method carried out a vibrational and buckling analysis of several composite sheets with variable fiber spacing subjected to in-plane boundary loading, Leissa and Martin [7] found exact solution for composites with variable fiber spacing under four different boundary conditions at four edges.

Rayleigh–Ritz method was also used by Pandy [8] for buckling analysis of composites with varying fiber spacing. Shiau and Chue [9] developed a technique to reduce interlaminar stresses at free edges by changing the fiber volume at those regions. A plane stress problem was solved by Shiau and Lee [10] for composite laminate with variable fiber spacing having a circular hole in it, subjected to in-plane boundary loading.

CHAPTER 2

JK-INTEGRAL FORMULATION FOR HYGROTHERMAL LOAD IN FIBROUS COMPOSITES WITH VARIABLE FIBER SPACING

2.1. Constitutive relations

Constitutive relations are defined with respect to material properties and initially formulate the reaction of the material subjected to loads. Defining these relations always involves definition of the category of the material. Elasticity of the material used in this study is the first thing to be mentioned, since our model is deformed only at the time of application of the loads. Homogenous materials are known as materials having the same properties at all point through material, thus changing material properties in x_2 direction makes this material non-homogenous. Orthotropic materials are materials having two planes of symmetry; such a characteristic fits properties of the material used in this study, consequently the composite sheet used is a non-homogenous orthotropic material. For such a material the hygrothermal constitutive relations of plane stress condition can be expressed as [31]:

$$\begin{pmatrix} \varepsilon_1 \\ \varepsilon_2 \\ 2\varepsilon_{12} \end{pmatrix} = \begin{bmatrix} \frac{1}{E_1} & -\frac{\nu_{12}}{E_1} & 0 \\ -\frac{\nu_{12}}{E_1} & \frac{1}{E_2} & 0 \\ 0 & 0 & \frac{1}{G_{12}} \end{bmatrix} \begin{pmatrix} \sigma_1 \\ \sigma_2 \\ \sigma_{12} \end{pmatrix} + \begin{pmatrix} \alpha_1 \\ \alpha_2 \\ 0 \end{pmatrix} \Delta T + \begin{pmatrix} \beta_1 \\ \beta_2 \\ 0 \end{pmatrix} \Delta c \tag{2.1.1}$$

In the equation above ε_{ij} are the strain tensor elements. σ_{ij} are stresses and ΔT and Δc are respectively thermal and moisture concentration differences at the point. This variation is calculated with respect to T_0 and c_0 , which are initial reference values causing no strain in the medium. α is the thermal expansion coefficient and β shows moisture expansion coefficient. Non-dimensional term, Moisture concentration is defined by the following formula [38]:

$$c = \lim_{\Delta V \to \infty} \frac{Mass\ of\ water\ absorbed\ in\ volume\ \Delta V}{Mass\ of\ dry\ material\ \ of\ volume\ \Delta V} \tag{2.1.2}$$

Moisture absorption in the composite causes swelling in the matrix, which causes strain and as a result stress in the structure similar to temperature. The microscopic interpretation of this phenomenon can be the capability of structure to capture water molecules thus gaining extra volume which causes strain in the structure. Hygrothermal expansion properties of some typical composite material are as below [39]:

Table2.1.1: Thermal and Hygroscopic expansion properties

Material	Thermal expansion coefficient (10^{-6} m/m)/C^0		Hygroscopic expansion coefficient (m/m)	
	α_1	α_2	β_1	β_2
AS Graphite/epoxy	0.88	31.0	0.09	0.30
E-glass/epoxy	6.3	20.0	0.014	0.29
AF-126-2 adhesive	29.0	29.0	0.20	0.20
1020 steel	12.0	12.0	-	-

Formulation of this two-dimensional anisotropic elasticity problem is carried out using $\phi(z_k)$, which is an analytic bi-harmonic function of complex variable z_k, known as Airy function that can be used in finding stress field, where,

$$z_k = x_k + y_k \tag{2.1.3}$$

$$x_k = x + \alpha_k y, \qquad y_k = \beta_k y, \qquad (k = 1,2) \tag{2.1.4}$$

α_k and β_k refer to real and imaginary part of $\mu_k = \alpha_k + i\beta_k$. μ_k can be found by finding roots of characteristic equation at the crack tip. $\overline{\mu_k}$ are conjugates of μ_k.

2.2. Jk-integral and the mechanical strain energy density function

For plane strain and plane stress conditions, J_k-integral formulation at the crack tip can be written as [30]:

$$J_k = \lim_{\Gamma\varepsilon \to 0} \left\{ \int_{\Gamma\varepsilon} \left(W n_k - \sigma_{ij} n_j u_{i,k} \right) ds \right\} \qquad (i,j,k = 1,2) \tag{2.2.1}$$

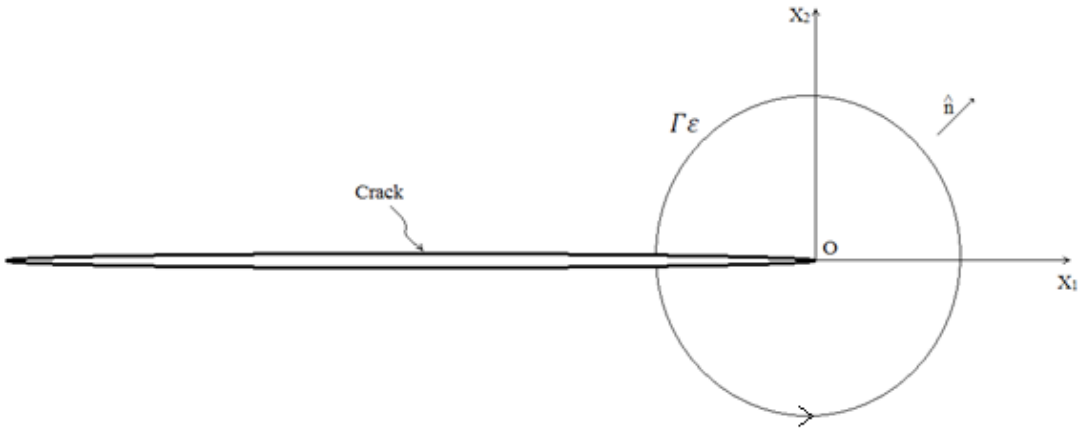

Figure2.2.1: Integration curve on the crack

In Eq.(2.2.1), Γ_ε represents an open curve, on which the integration is calculated, illustrated in figure-2.2.1. The integration curve starts on the lower crack surface and ends on the upper one. In the equation n_k, σ_{ij} and s represent outward unit vector, stress tensor and arc length respectively. u_i stand for displacement units, whereas $u_{i,k}$ represents differentiations, i.e. $(\,)_k \equiv \frac{\partial(\,)}{\partial x_k}$. W is the mechanical strain energy density function and defined as:

$$W = \begin{cases} \frac{1}{2}\sigma_{ij}\varepsilon_{ij}^m & \text{for plane stress} \\ \frac{1}{2}\sigma_{ij}\varepsilon_{ij}^m + \frac{1}{2}\sigma_{33}\varepsilon_{33}^m & \text{for plane strain} \end{cases} \tag{2.2.2}$$

ε_{ij}^m is the mechanical strain, so considering Eq.(2.2.1), we can say:

$$\varepsilon_{11}^m = \varepsilon_{11} - \alpha_1 \Delta T - \beta_1 \Delta c \tag{2.2.3a}$$

$$\varepsilon_{22}^m = \varepsilon_{22} - \alpha_2 \Delta T - \beta_2 \Delta c \tag{2.2.3b}$$

$$\varepsilon_{12}^m = \varepsilon_{12} \tag{2.2.3c}$$

Using Eq.(2.2.2) and Eq.(2.2.3) for plane stress we can conclude [31]:

$$W = \frac{E_1^2(\varepsilon_{11} - \alpha_1\Delta T - \beta_1\Delta c) + \nu_{12}E_1E_2(\varepsilon_{22} - \alpha_2\Delta T - \beta_2\Delta c)}{2(E_1 - \nu_{12}^2E_2)}(\varepsilon_{11} - \alpha_1\Delta T - \beta_1\Delta c) + \frac{\nu_{12}E_1E_2(\varepsilon_{11} - \alpha_1\Delta T - \beta_1\Delta c) + E_1E_2(\varepsilon_{22} - \alpha_2\Delta T - \beta_2\Delta c)}{2(E_1 - \nu_{12}^2E_2)}(\varepsilon_{22} - \alpha_2\Delta T - \beta_2\Delta c) + 2G_{12}\varepsilon_{12}^2 \quad (2.2.4)$$

Solution of J_k-Integral indicated in Eq.(2.2.1) involves solution of another integral Eq.(2.2.5) defined on close curve Γ. Figure-2.2.2 shows curve Γ, which according to Eq.(2.2.6) consists of four open curves.

$$I_k = \oint_\Gamma (\sigma_{ij}u_{i,k} - W\delta_{kj})qn_j \, d\Gamma \qquad (i,j,k = 1,2) \quad (2.2.5)$$

$$\Gamma = \Gamma_0 + \Gamma_e + \Gamma_{cr}^- + \Gamma_{cr}^+ \quad (2.2.6)$$

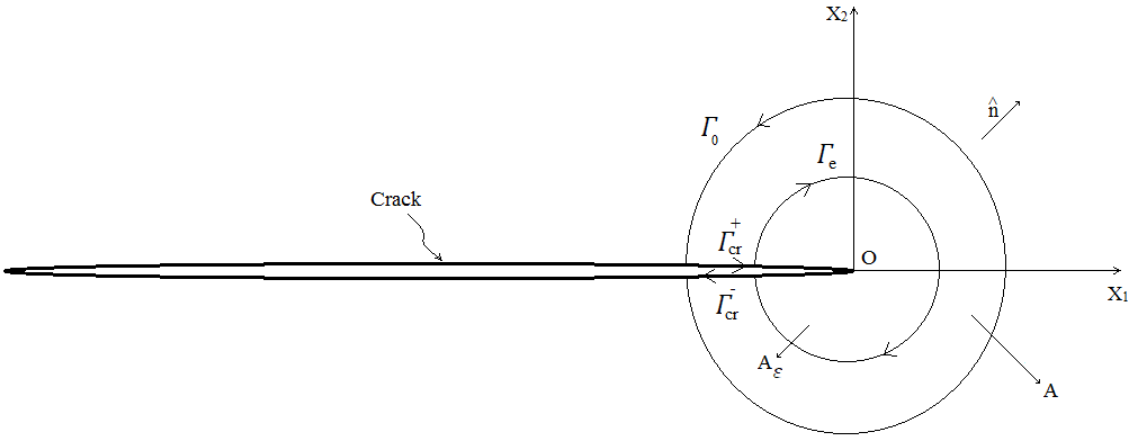

Figure 2.2.2: Illustration of Γ close curve at crack tip

I_k-integral is defined over Γ and can be converted to an integral over Area A as Eq.(2.2.6). For this conversion divergence theorem was manipulated (Further information for this theory can be found in APPENDIX A)

$$I_k = \iint_A \frac{\partial}{\partial x_j}(\sigma_{ij}u_{i,k}q - W\delta_{kj}q)dA \quad (2.2.7)$$

From equations of equilibrium it's known that:

$$\sigma_{ij,j} = 0 (i, j = 1,2) \tag{2.2.8}$$

To further ease calculations integrand of $I_k$as Z_k:

$$Z_k = \frac{\partial}{\partial x_j}\left(\sigma_{ij} u_{i,k} q - \delta_{kj} q\right) \quad (i, j, k = 1,2) \tag{2.2.9}$$

Differentiating the elements of Eq.(2.2.8), changes it to:

$$Z_k = \left(\sigma_{ij,j} u_{i,k} + \sigma_{ij} u_{i,kj} - W_{,j}\delta_{kj} - W\delta_{kj,j} - W\delta_{kj,j}\right)q + \left(\sigma_{ij} u_{i,k} - W\delta_{kj}\right)q_{,j} \quad (i, j, k = 1,2) \tag{2.2.10}$$

Kronecker's delta function has the property as Eq.(2.2.11):

$$\delta_{kj,j} = 0 \tag{2.2.11}$$

Using property of Kronecker's delta in equation Eq.(2.2.10):

$$W_{,j}\delta_{kj} = W_{,k} \tag{2.2.12}$$

Dividing Z_k into two parts:

$$Z_k^I = \left(\sigma_{ij,j}u_{i,k} + \sigma_{ij}u_{i,kj} - W_{,j}\delta_{kj} - W\delta_{kj,j} - W\delta_{kj,j}\right)q \tag{2.2.13}$$

$$Z_k^{II} = \left(\sigma_{ij}u_{i,k} - W\delta_{kj}\right)q_{,j} \tag{2.2.14}$$

For calculation of components of Z_k we need to find derivative of W as below:

$$W_{,k} = \frac{\partial W}{\partial x_k} = \frac{\partial W}{\partial \varepsilon_{ij}}\frac{\partial \varepsilon_{ij}}{\partial x_k} + \left(\frac{\partial W}{\partial x_k}\right)_{expl} \tag{2.2.15}$$

For Hygrothermal boundary conditions explicit part of $W_{,k}$ would be:

$$\begin{aligned}\left(\frac{\partial W}{\partial x_k}\right)_{expl} = {} & \frac{\partial W}{\partial E_1}\frac{\partial E_1}{\partial x_k} + \frac{\partial W}{\partial E_2}\frac{\partial E_2}{\partial x_k} + \frac{\partial W}{\partial G_{12}}\frac{\partial G_{12}}{\partial x_k} + \frac{\partial W}{\partial \nu_{12}}\frac{\partial \nu_{12}}{\partial x_k} + \\ & \frac{\partial W}{\partial \alpha_1}\frac{\partial \alpha_1}{\partial x_k} + \frac{\partial W}{\partial \alpha_2}\frac{\partial \alpha_2}{\partial x_k} + \frac{\partial W}{\partial \beta_1}\frac{\partial \beta_1}{\partial x_k} + \frac{\partial W}{\partial \beta_2}\frac{\partial \beta_2}{\partial x_k} + \\ & \frac{\partial W}{\partial \Delta T}\frac{\partial \Delta T}{\partial x_k} + \frac{\partial W}{\partial \Delta c}\frac{\partial \Delta c}{\partial x_k} \qquad (k = 1,2)\end{aligned} \tag{2.2.16}$$

From Eq.(2.2.2) we can obtain the following equation:

$$\frac{\partial W}{\partial \varepsilon_{ij}} = \sigma_{ij} \tag{2.2.17}$$

We also know that:

$$\varepsilon_{ij} = \frac{1}{2}(u_{i,j} + u_{j,i}) \tag{2.2.18}$$

Changing the expression mode of $W_{,k}$ following equations can be achieved:

$$W_{,k} = \sigma_{ij}\frac{1}{2}\frac{\partial}{\partial x_k}\left(\frac{\partial u_i}{\partial x_j} + \frac{\partial u_j}{\partial x_i}\right) + \left(\frac{\partial W}{\partial x_k}\right)_{expl} \qquad (i,j,k = 1,2) \tag{2.2.19}$$

$$W_{,k} = \sigma_{ij}\frac{1}{2}\frac{\partial}{\partial x_k}\frac{\partial u_i}{\partial x_j} + \sigma_{ij}\frac{1}{2}\frac{\partial}{\partial x_k}\frac{\partial u_i}{\partial x_i} + \left(W_{,k}\right)_{expl} \qquad (i,j,k = 1,2) \tag{2.2.20}$$

$$W_{,k} = \sigma_{ij}u_{i,kj} + \left(W_{,k}\right)_{expl} \qquad (i,j,k = 1,2) \tag{2.2.21}$$

Then Z_k^I can be expressed as:

$$Z_k^I = \left(\sigma_{ij,j}u_{i,k} - \left(W_{,k}\right)_{expl}\right)q \qquad (i,j,k = 1,2) \tag{2.2.22}$$

And considering Eq.(2.2.8):

$$Z_k^I = -\left(W_{,k}\right)_{expl}q \tag{2.2.23}$$

Consequently Z_k can be written as:

$$Z_k = -\left(W_{,k}\right)_{expl}q + \left(\sigma_{ij}u_{i,k} - W\delta_{kj}\right)q_{,j} \qquad (i,j,k = 1,2) \tag{2.2.24}$$

Using previous equations I_k integral in Eq.(2.2.5):

$$I_k = \iint_A \left(\sigma_{ij} u_{i,k} - W\delta_{kj}\right) q_{,j}\, dA - \iint_A \left(W_{,k}\right)_{expl} q\, dA \tag{2.2.25}$$

For simplicity of expression b_k is defined as:

$$b_k = \left(\sigma_{ij} u_{i,k} - W\delta_{kj}\right) q n_j \tag{2.2.26}$$

Thus I_k can be simplified as:

$$I_k = \oint_\Gamma b_k\, d\Gamma = \oint_{\Gamma_0} b_k\, d\Gamma + \oint_{\Gamma_{cr}^-} b_k\, d\Gamma + \oint_{\Gamma_{cr}^+} b_k\, d\Gamma + \oint_{\Gamma_e} b_k\, d\Gamma, \quad (k = 1,2) \tag{2.2.27}$$

q is an conventional function of x_1 and x_2, equal to zero on the boundary of A and equal to one at the crack tip. In our analysis for simplicity a right circular cone is used as the function:

$$q(x_1, x_2) = 1 - \frac{\sqrt{x_1^2 + x_2^2}}{R} \tag{2.2.28}$$

So first integral of I_k is equal to zero because the integration is on the Γ_0 domain, where q is equal to zero:

$$I_k = \oint_\Gamma b_k\, d\Gamma = -\oint_{\Gamma_e} b_k\, d\Gamma + \oint_{\Gamma_{cr}^-} b_k\, d\Gamma + \oint_{\Gamma_{cr}^+} b_k\, d\Gamma \tag{2.2.29}$$

So substituting b_k we have:

$$\oint_{\Gamma} b_k d\Gamma = \oint_{\Gamma_e} \left(W\delta_{kj} - \sigma_{ij}u_{i,k}\right)qn_j \, d\Gamma + \oint_{\Gamma_{cr}^{+}} b_k \, d\,\Gamma + \oint_{\Gamma_{cr}^{-}} b_k \, d\Gamma \qquad (i,j,k = 1,2) \tag{2.2.30}$$

As it can be perceived from Eq.(2.3.31) first integral is equal to J_k-integral, so:

$$J_k = \iint_A \left(\sigma_{ij}u_{i,k} - W\delta_{kj}\right)q_{,j} \, dA - \iint_A \left(W_{,k}\right)_{expl} q dA - \int_{\Gamma_{cr}^{+}} \left(\sigma_{ij}u_{i,k} - W\delta_{kj}\right)qn_j \, d\Gamma - \int_{\Gamma_{cr}^{-}} \left(\sigma_{ij}u_{i,k} - W\delta_{kj}\right)qn_j \, d\Gamma \quad (i,j,k = 1,2) \tag{2.2.31}$$

We know that crack surfaces are free and no stress is present on them, so on crack faces, which equal to Γ_{cr}^{+} and Γ_{cr}^{-} domains:

$$\sigma_{ij}u_{i,k}n_j = 0 \tag{2.2.32}$$

Applying Eq.(2.2.32) in Eq.(2.2.31):

$$J_k = \iint_A \left(\sigma_{ij}u_{i,k} - W\delta_{kj}\right)q_{,j} \, dA - \iint_A \left(W_{,k}\right)_{expl} q \, dA + \int_{\Gamma_{cr}^{+}} (W^{+}n_k^{+})q \, d\Gamma + \int_{\Gamma_{cr}^{-}} (W^{-}n_k^{-})q \, d\Gamma \quad (i,j,k = 1,2) \tag{2.2.33}$$

Since, $n_k^{-} = -n_k^{+}$:

$$J_k = \iint_A \left(\sigma_{ij}u_{i,k} - W\delta_{kj}\right)q_{,j} \, dA - \iint_A \left(W_{,k}\right)_{expl} q \, dA + \int_{\Gamma_{cr}} (W^{+} - W^{-})qn_k^{+} \, d\Gamma \quad (i,j,k = 1,2) \tag{2.2.34}$$

From Eq.(2.2.34), also considering that on Γ_{cr}^{+} and Γ_{cr}^{-}, n_1 is equal to zero, we can write components of J_k-integral over a definite finite domain as:

$$J_1 = \iint_A \left(\sigma_{ij} u_{i,1} - W\delta_{1j}\right) q_{,j} dA - \iint_A \left(W_{,1}\right)_{expl} q dA \qquad (i,j = 1,2) \tag{2.2.35}$$

$$J_2 = \iint_A \left(\sigma_{ij} u_{i,2} - W\delta_{2j}\right) q_{,j} dA - \iint_A \left(W_{,2}\right)_{expl} q dA - \int_{\Gamma_{cr}} (W^{+} - W^{-}) q ds \qquad (i,j = 1,2) \tag{2.2.36}$$

So the integration domain is changed to an area integral A and a line integral Γ_{cr}. Presentation of the integral domain in figure-2.2.3 shows, that Γ_{cr} is actually the crack length surrounded by area A. The shape and the size of the area of the integration should not affect the result of the solution, because this formulation is independent of the domain. In the solution, for validation of this property of the formulation, several circular areas are considered as the integration area.

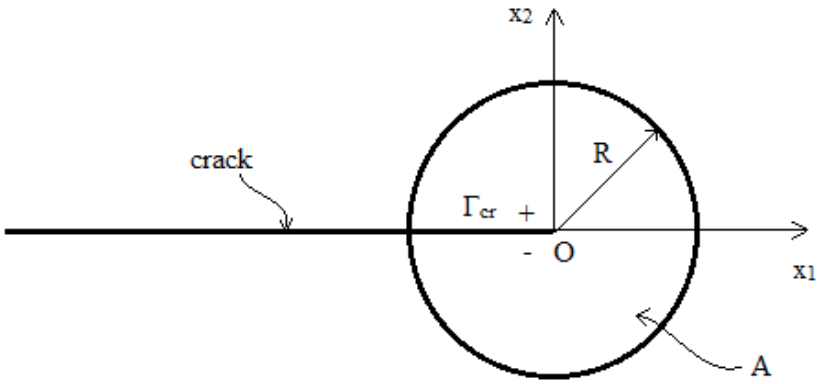

Figure2.2.3: New integration domains after the change by divergence theorem

W^{+} and W^{-}resembles to the strain energy density on the upper and lower face of the crack respectively, figure-2.2.3.

Having defined all the elements of Eq.(2.2.35) and Eq.(2.2.36), the solution of the integrals were processed using standard Gauss quadrature, but the only problem with the integral calculation was discontinuity for the $(W^+ - W^-)$ in J_2 expression. The solution for this difficulty was presented by Eischen [30], suggesting use of discrete integration on the domain and division of integration interval into two parts, one part is the interval far from crack tip, and the other one would be near crack tip which includes the singularity on the domain. The solution for the second part was reached using asymptotic approximation for mechanical strain energy density difference. The Illustrtion of d as a measurement for determining the close and far parts of the domain is presented in figure-2.2.4.

$$\int_{\Gamma_{cr}} (W^+ - W^-)q \, d\Gamma = \int_0^R (W^+ - W^-)q \, ds = \int_0^{R-d} (W^+ - W^-)q \, ds + \int_{R-d}^R (W^+ - W^-)q \, ds \tag{2.2.37}$$

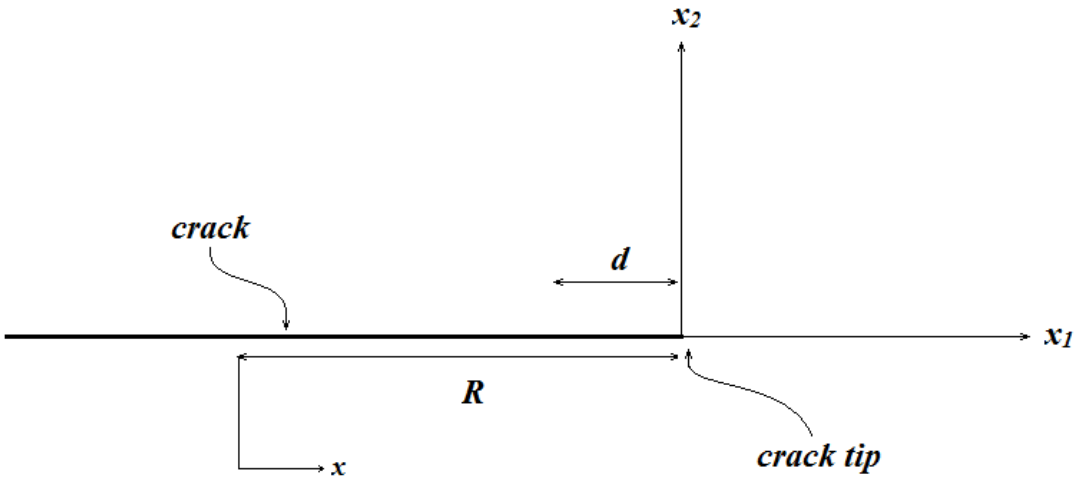

Figure 2.2.4: Representation of d in the model geometry

In order to find the solution for the integral near crack tip, asymptotic distribution of stresses is required in this region. These stresses are defined as below [29]:

$$\sigma_{ij}(r,\theta) = \frac{K_I}{\sqrt{2\pi r}} f_{ij}^1(\theta) + \frac{K_{II}}{\sqrt{2\pi r}} f_{ij}^{II}(\theta) + T_{str}\delta_{1i}\delta_{1j} \quad (i,j = 1,2) \tag{2.2.38}$$

$$\sigma_{11}(r,\theta) = \frac{K_I}{\sqrt{2\pi r}} Re\left[\frac{\mu_1\mu_2}{\mu_1-\mu_2}\left(\frac{\mu_2}{\sqrt{cos\theta+\mu_2 sin\theta}} - \frac{\mu_1}{\sqrt{cos\theta+\mu_1 sin\theta}}\right)\right] + \frac{K_{II}}{\sqrt{2\pi r}} Re\left[\frac{1}{\mu_1-\mu_2}\left(\frac{(\mu_2)^2}{\sqrt{cos\theta+\mu_2 sin\theta}} - \frac{(\mu_1)^2}{\sqrt{cos\theta+\mu_1 sin\theta}}\right)\right] + T_s \quad (2.2.39)$$

$$\sigma_{22}(r,\theta) = \frac{K_I}{\sqrt{2\pi r}} Re\left[\frac{1}{\mu_1-\mu_2}\left(\frac{\mu_1}{\sqrt{cos\theta+\mu_2 sin\theta}} - \frac{\mu_2}{\sqrt{cos\theta+\mu_1 sin\theta}}\right)\right] + \frac{K_{II}}{\sqrt{2\pi r}} Re\left[\frac{1}{\mu_1-\mu_2}\left(\frac{1}{\sqrt{cos\theta+\mu_2 sin\theta}} - \frac{1}{\sqrt{cos\theta+\mu_1 sin\theta}}\right)\right] \quad (2.2.40)$$

$$\sigma_{12}(r,\theta) = \frac{K_I}{\sqrt{2\pi r}} Re\left[\frac{\mu_1\mu_2}{\mu_1-\mu_2}\left(\frac{1}{\sqrt{cos\theta+\mu_1 sin\theta}} - \frac{1}{\sqrt{cos\theta+\mu_2 sin\theta}}\right)\right] + \frac{K_{II}}{\sqrt{2\pi r}} Re\left[\frac{1}{\mu_1-\mu_2}\left(\frac{\mu_1}{\sqrt{cos\theta+\mu_1 sin\theta}} - \frac{\mu_2}{\sqrt{cos\theta+\mu_2 sin\theta}}\right)\right] \quad (2.2.41)$$

In equations above r and θ are the polar coordinates presented in figure-2.2.5.

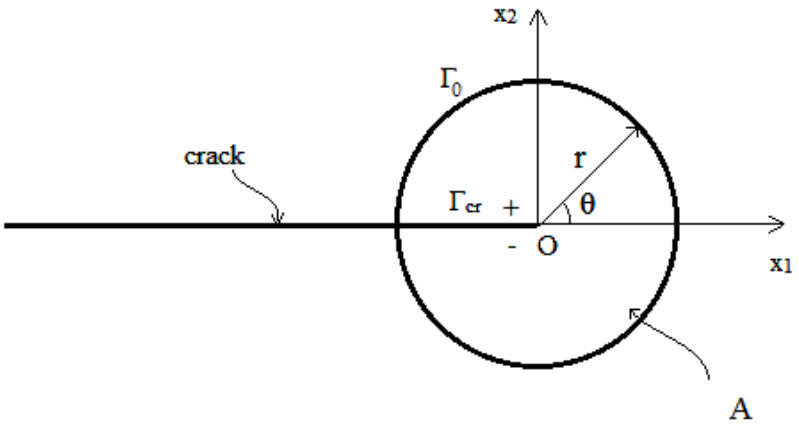

Figure 2.2.5: Polar coordination at crack tip

Expression of difference of W function in polar coordinates would be:

$$W^+ - W^- = W(r,\pi) - W(r,-\pi) \quad (2.2.42)$$

From Eq.(2.2.2), Eq.(2.2.39) and Eq.(2.2.42):

$$W(r,\pi) - W(r,-\pi) = (W^+ - W^-) = \frac{1}{2}\left[a_{11}(\frac{4K_{II}}{\sqrt{2\pi r}}[D(\beta_1^2 - \beta_2^2)]T_s)\right] \tag{2.2.43}$$

For simplicity of equations L is defined as:

$$L = 2a_{11}K_{II}[D(\beta_1^2 - \beta_2^2)]T_s \tag{2.2.44}$$

β's refer to those in Eq.(2.1.3), then Eq.(2.2.43) turns to:

$$(W^+ - W^-) = \frac{1}{\sqrt{2\pi r}}L \tag{2.2.45}$$

Defining following parameters:

$$a_{11} = \frac{1}{E_1} \tag{2.2.46}$$

$$D = -\frac{1}{\beta_1 - \beta_2} \tag{2.2.47}$$

Then Eq.(2.2.37) can be written as:

$$\int_{\Gamma_c}(W^+ - W^-)q\, d\Gamma \approx \int_0^{R-d}(W^+ - W^-)q\, ds + \int_{R-d}^{R}\frac{L}{\sqrt{2\pi r}}q\, ds \tag{2.2.48}$$

Simply solving last part of the integral in Eq.(2.2.48), following equation is obtained:

$$\begin{aligned} J_2 = &\iint_A (\sigma_{ij}u_{i,2} - W\delta_{2j})q_{,j}dA - \iint_A (W_{,2})_{expl}qdA \\ &- \int_0^{R-d}(W^+ - W^-)qds + 4\sqrt{\frac{d}{2\pi}}\frac{b(3R-d)}{3R}K_{II}T_s(i,j=1,2) \end{aligned} \tag{2.3.49}$$

In Eq.(2.2.49), R is length of the path, integration is calculated over, as shown in figure-2.2.3, the path near to the crack tip, over which the asymptotic approximation of $(W^+ - W^-)$ is substituted in the main equation, is represented as d, figure-2.2.5 shows the dimensions in the model. $K_{II}$is mode II stress intensity factor and T_s stands for T-stress.b is equal to $Im(\mu_1 + \mu_2)$. μ_1 and μ_2 are roots of characteristic equation below [29]:

$$a_{11}\mu^4 + (2a_{12} + a_{66})\mu^2 + a_{22} = 0 \tag{2.2.50}$$

In the equation above the constants are equal to the terms below:

$$a_{11} = \frac{1}{E_1}, \quad a_{12} = -\frac{\nu_{12}}{E_1}, \quad a_{22} = \frac{1}{E_2}, \quad a_{66} = \frac{1}{G_{12}} \tag{2.2.51}$$

2.3. Computation of the crack parameters using Jk-integral formulation

Considering the final form of J_2 formulation in Eq.(2.2.49),It can be distinguished from equation that the solution can't be achieved by solving the integral, because K_I, K_{II} and T_s are unknown. In order to find T_s, K_I and K_{II}, a new form of the equation is presented for $\widetilde{J_2}$ [30]:

$$\widetilde{J_2}^1 = J_2 - \sqrt{d_1}\left[1 - \frac{d_1}{3R}\right]S \tag{2.3.1}$$

$$\widetilde{J_2}^2 = J_2 - \sqrt{d_2}\left[1 - \frac{d_2}{3R}\right]S \tag{2.3.2}$$

Equations above are $\widetilde{J_2}$ written for two different values of d, which allow us to evaluate the values of S and J_2 through a linear equation system. The values given to d where defined dependent on the crack length and these values are equal to $d_1 = 0.0001a$ and $d_2 = 0.0002a$. In this simplified equations the approximation is presented in terms of one variable:

$$S = \frac{4Im(\mu_1 + \mu_2)a_{11}}{\sqrt{2\pi}} K_{II} T_s \tag{2.3.3}$$

Then solution for S and J_2 would be:

$$J_2 = \frac{\sqrt{d_1}\left(1-\frac{d_1}{3R}\right)\tilde{J_2}^2 - \sqrt{d_2}\left(1-\frac{d_2}{3R}\right)\tilde{J_2}^2}{\sqrt{d_1}\left(1-\frac{d_1}{3R}\right) - \sqrt{d_2}\left(1-\frac{d_2}{3R}\right)} \tag{2.3.4}$$

$$S = \frac{\tilde{J_2}^1 - \tilde{J_2}^2}{\sqrt{d_1}\left(1-\frac{d_1}{3R}\right) - \sqrt{d_2}\left(1-\frac{d_2}{3R}\right)} \tag{2.3.5}$$

After getting S and J_2, T-stress can be calculated from Eq.(2.2.44), Eq.(2.2.45), Eq.(2.2.47) and Eq.(2.3.3):

$$T_s = \frac{S\sqrt{2\pi}}{4a_{11}K_{II}D(\beta_1^2 - \beta_2^2)} \tag{2.3.6}$$

Since J_1 and $\tilde{J_2}$are solved only using numerical method for the integral, and solving the equation system, we obtain $J_2$and S. As an additional equation, to make system of the unknowns solvable, we use the relation between J_1 and J_2 [29]:

$$J_1 = B_1K_I^2 + B_2K_{II}^2 \tag{2.3.4}$$

$$J_2 = B_3K_IK_{II} \tag{2.3.5}$$

Eq.(2.3.4) and Eq.(2.3.5) clearly show that K_I and K_{II} are coupled, so this system of equations for intensity factors can be solved using numerical methods. Kim and Paulino [29] have used Newton iteration method to find intensity factors, but in this method they needed to have initial values for SIFs. These initial values were obtained using DCT (Displacement Correlation Technique). However, in this study the values for μ_k were all purely imaginary, because directions of axes coincide with principle directions of elasticity and crack is laying on one of the principle orthotropy directions.

In the Eq.(2.3.4) and Eq.(2.3.5) and B_1 , B_2 and B_3 would be dependent on material properties of the medium and are defined as:

$$B_1 = -\frac{a_{11}}{2}Im\{(\mu_1+\mu_2)\overline{\mu_1\mu_2}\} = \frac{a_{11}}{2}(\beta_1+\beta_2)(\beta_1\beta_2) \tag{2.3.6}$$

$$B_2 = \frac{a_{11}}{2}Im\{\mu_1+\mu_2\} = \frac{a_{11}}{2}(\beta_1+\beta_2) \tag{2.3.7}$$

$$B_3 = \frac{a_{11}}{4}Im\{\mu_1\mu_2(\mu_1+\mu_2+\overline{\mu_1}+\overline{\mu_2}) + (\mu_1+\mu_2)(\mu_1\mu_2+3\overline{\mu_1\mu_2})\} = -a_{11}(\beta_1+\beta_2)(\beta_1\beta_2) \tag{2.3.8}$$

$\overline{\mu_1}$ and $\overline{\mu_2}$ are representing the conjugates of μ_1 and μ_2 in the equation. Defining K_I in terms of K_{II}, one can write:

$$K_I = -\frac{J_2}{K_{II} a_{11}(\beta_1 + \beta_2)\beta_1\beta_2} \tag{2.3.9}$$

Now we can write relation between intensity factors as a forth degree equation which can be changed to second degree equation:

$$K_{II}^4 - \frac{2J_1}{a_{11}(\beta_1 + \beta_2)} K_{II}^2 + \left(-\frac{J_2}{a_{11}(\beta_1 + \beta_2)\beta_1\beta_2}\right)^2 \beta_1\beta_2 = 0 \tag{2.3.10}$$

If consider:

$$K_{II}^2 = F \tag{2.3.11}$$

Then Eq.(2.3.10) becomes:

$$F^2 - \frac{2J_1}{a_{11}(\beta_1 + \beta_2)} F + \left(-\frac{J_2}{a_{11}(\beta_1 + \beta_2)\beta_1\beta_2}\right)^2 \beta_1\beta_2 = 0 \tag{2.3.12}$$

Solving the equation above:

$$F = \frac{J_1}{a_{11}(\beta_1 + \beta_2)}\left(1 \pm \sqrt{1 - \left(\frac{J_2}{J_1}\right)^2 \frac{1}{\beta_1\beta_2}}\right) \tag{2.3.13}$$

Then according to Eq.(2.3.11) and Eq.(2.3.9):

$$K_I = \pm\sqrt{\frac{J_1}{2B_1}\left\{1 \pm \sqrt{1 - \frac{4B_1B_2}{B_3^2}\left(\frac{J_2}{J_1}\right)^2}\right\}} \tag{2.3.14}$$

$$K_{II} = \frac{J_2}{B_3 K_I} \tag{2.3.15}$$

Once K_{II} is calculated from the equation above T-stress can be determined using Eq.(2.3.6). In order to determine the right sign for the intensity factors, a method based on relative normal and tangential displacements of two nodes, defined very close to the crack tip was manipulated [26]. Investigating displacements of nodes close to crack tip will truly show if either – or + sign should be assigned for intensity factors. Two couples of nodes at both upper and lower crack faces were chosen, then [29]:

$$\Delta_1 = u_2^+ - u_2^- \tag{2.3.16}$$

$$\Delta_2 = u_1^+ - u_1^- \tag{2.3.17}$$

A positive outcome for Δ_1 implies that K_I should be positive, which shows crack is open, and if Δ_2 is positive K_{II} should be positive too. In Eq.(2.3.14) and Eq.(2.3.15), the signs in the parenthesis should also be determined [31]:

If $|\Delta_1| \geq |\Delta_2|$ take + for K_{II} and – for K_I

If $|\Delta_1| \leq |\Delta_2|$ take - for K_{II} and + for K_I

CHAPTER 3

FINITE ELEMENT IMPLEMENTATION

Complexity of problems in structural and elasticity analysis was the first motivation for invention of finite element method (FEM). FEM is used in variety of analysis, but they all have a certain characteristic in common, and it's discretizing meshes of a continuous domain and making a sort of sub-domains.

The finite element method as a numerical method to calculate fracture parameters of the medium was used for implementation of the J_k-integral method processed in chapter 2. ANSYS [37] as a general purpose finite element program was employed to process algorithm written in ANSYS macro language. Using finite element to find desired fracture parameter on a medium had definite procedure. Firstly simulated model had to be meshed. Meshing involved a special design especially around crack tip, since a good meshing can increase your result accuracy a great deal. In the second step the using mechanical properties of the composite, properties of elements in the medium were determined (this part of the code is available in Appendix C). Having determined properties of the material, thermal and hygroscopic loads were defined over the model boundaries. Structural constraints of the medium were also defined. This was the end of preprocessing part of the problem which was totally written as APDL code in ANSYS. Equations for determining nodal hygrothermal loads were solved and were transformed to structural load on nodes. Post-processing the results provided essential requirements for calculation of fracture parameters. Expression of details of these procedures and finite element application details are the objective of this section.

In order to find fracture parameters of the crack, temperature and moisture concentration in distribution at all points of the medium should be known. To determine thermal field in the model for steady-state heat flow case in the fibrous composite sheet the Eq.(3.1) was solved by ANSYS.

$$\frac{\partial}{\partial x_1}\left(k_1(x_2)\frac{\partial T}{\partial x_1}\right)+\frac{\partial}{\partial x_2}\left(k_2(x_2)\frac{\partial T}{\partial x_2}\right)=0 \tag{3.1}$$

$k_1$and k_2 are only a function of fiber volume and consequently a function of only $x_2$as explained in Eq.(2.2.1e), and representing thermal conductivity in x_1 and x_2 directions respectively.For calculation of the moisture diffusion field a similar partial differential equation was also solved by ANSYS Eq.(3.2).

$$\frac{\partial}{\partial x_1}\left(D_1(x_2)\frac{\partial c}{\partial x_1}\right)+\frac{\partial}{\partial x_2}\left(D_2(x_2)\frac{\partial c}{\partial x_2}\right)=0 \tag{3.2}$$

Similar to k's in Eq.(3.1), D_1 and D_2 are only a function of fiber volume and consequently a function of only x_2 as explain in Eq.(2.2.1f), and representing mass diffusivity in x_1 and x_2 directions respectively.

After obtaining the nodal thermal and moisture concentration value for the model, structural analysis was carried out using ANSYS software, thus strain and stress distribution and also displacement nodal

values were determined by these solutions. The next step was to use these nodal results in numerical calculation of J_k-integral and finally finding the fracture parameter using the results of the numerical integral solution.

It's clear that J_k-integral is quite complex to be evaluated exactly, finding approximate solution using numerical methods is the main object of the numerical analysis of this study. In order to be able to find the approximate values for integrals it's essential to find the most appropriate with sufficient degree polynomial to be used in numerical method as approximation for the integrand.

If the integral to be calculated with this numerical method is considered to be:

$$\Pi = \int_{x_1}^{x_2} F(x)dx \tag{3.3}$$

Approximated $f(x)$ by using $w(x)$ can be written as:

$$F(x) \approx \sum_{i=1}^{N} F_i \, \psi_i(x) \tag{3.4}$$

F_i is value of $F(x)$ at the i^{th}point of interval and $\psi_i(x)$are polynomials of degree $N-1$.

Quadrature formula is expressed as:

$$A = \int_{x_1}^{x_2} F(x)dx \approx \sum_{i=1}^{r} F(x_i) \, W_i \tag{3.5}$$

Where, x_i, W_i are quadrature points and quadrature weights respectively.

Meshing and discretizing the domain various elements with quadrilateral shape are produced. The main problem with using these elements is complexity of shape functions and difficulty in calculation of integral over them. For convenience quadrilateral elements are transferred from global coordination system (x, y) to a local coordination system (ξ, η), thus their shape changes to simple rectangular. In this transformation the interval on which rectangle is defined and shown as $\hat{A}$ in figure-3.1, changes to [-1, 1] for all the elements in local coordination system, considering that origin of the system is at the center of the element. In this study Gauss-Legendre quadrature is used as the numerical method for evaluation of J_k-integral.

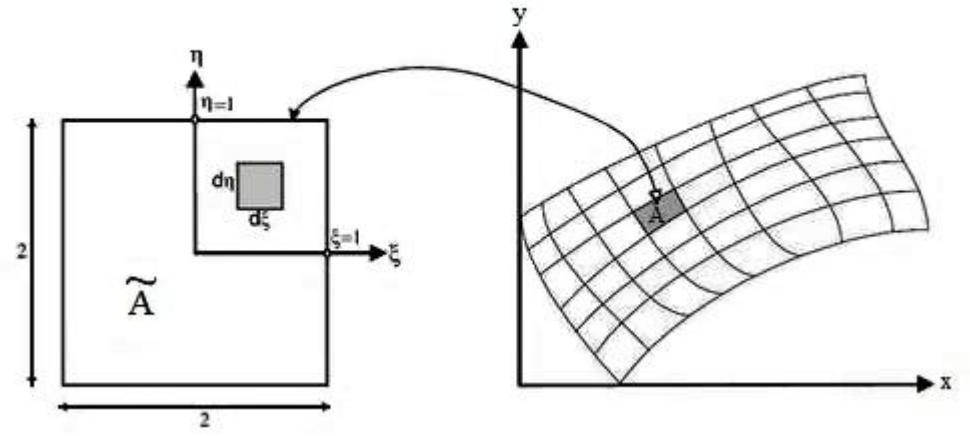

Figure 3.1: Transformation of quadrilateral element in (x, y)coordination system to master element in (ξ, η) coordination system

Coordination transformation between two coordination systems is done as follows:

$$x = \sum_{i=1}^{m} x_i \psi_i(\xi, \eta) \tag{3.6}$$

$$y = \sum_{i=1}^{m} y_i \psi_i(\xi, \eta) \tag{3.7}$$

In the equations above $\psi_i(\xi, \eta)$are known as shape functions. Similarly, the dependent variables that are intended to be found also can be approximated and written in the form of Eq.(3.6) and Eq.(3.7).

$$u(\xi, \eta) = \sum_{i=1}^{n} u_i \tilde{\psi}_i(\xi, \eta) \tag{3.8}$$

$\tilde{\psi}_i$ used in Eq.(3.8) may not be the same as $\psi_i$used in Eq.(3.7) and Eq.(3.6).

Approximation used for in equations above may be from different orders. If $m > n$ approximation used for geometry is higher order than dependent variable and called a Super-parametric case, If $m = n$ then they have the same order and called Isoparametric case, and if $m < n$ dependent variable has a higher order approximation. In this study isoparametric formulation were used.

As mentioned before Gauss-Legendre Quadrature was used in this study. The process of implementation for a line integral would be:

$$\int_a^b F(x)dx = \int_{-1}^{1} \hat{F}(\xi)d\xi = \sum_{i=1}^{r} \hat{F}(\xi_i)w_i \tag{3.9}$$

$$\hat{F}(\xi) = F\big(x(\xi)\big)J(\xi) \tag{3.10}$$

$$dx = Jd\xi \tag{3.11}$$

$$J = \sum_{i=1}^{m} x_i \frac{d\psi_i}{d\xi} \tag{3.12}$$

In equations above $r$and $w_i$are base points and weight factors respectively.

Gauss-Legendre Quadrature can be extended for area integrals:

$$\int_A F(x,y)dxdy = \int_A \hat{F}(\xi,\eta)d\xi d\eta = \int_{-1}^{1}\left[\int_{-1}^{1} \hat{F}(\xi,\eta)d\xi\right]d\eta \approx \int_{-1}^{1}\left[\sum_{i=1}^{N} \hat{F}(\xi_i,\eta)w_i\right]d\eta \approx \sum_{j=1}^{M}\sum_{i=1}^{N} \hat{F}\big(\xi_i,\eta_j\big)w_i\, w_j \tag{3.13}$$

$$\hat{F}(\xi,\eta) = F(x(\xi),y(\eta))|J| \tag{3.14}$$

$$dxdy = |J|d\xi d\eta \tag{3.15}$$

J is known as Jacobian matrix and used for transformations between coordinate systems and $|J|$is determinant of J. Jacobian matrix is defined as Eq.(3.16):

$$[J] = \begin{bmatrix} \frac{\partial x}{\partial \xi} & \frac{\partial y}{\partial \xi} \\ \frac{\partial x}{\partial \eta} & \frac{\partial y}{\partial \eta} \end{bmatrix} = \begin{bmatrix} \sum x_i \frac{\partial \psi_i}{\partial \xi} & \sum y_i \frac{\partial \psi_i}{\partial \xi} \\ \sum x_i \frac{\partial \psi_i}{\partial \eta} & \sum y_i \frac{\partial \psi_i}{\partial \eta} \end{bmatrix} \tag{3.16}$$

And determinant would be:

$$|J| = \frac{\partial x}{\partial \xi}\frac{\partial y}{\partial \eta} - \frac{\partial x}{\partial \eta}\frac{\partial y}{\partial \xi} \tag{3.17}$$

Second order Gauss-Legendre Quadrature was used in this study. For line and area integrals we have different Gauss points and weight points as follows:

$$\begin{cases} (\xi_i, \eta_j) = \left(\pm\frac{1}{\sqrt{3}}, -1\right) \\ w_i = 1 \end{cases} \tag{3.18}$$

$$\begin{cases} (\xi_i, \eta_j) = \left(\pm\frac{1}{\sqrt{3}}, \pm\frac{1}{\sqrt{3}}\right) \\ w_i = 1, \;\; w_j = 1 \end{cases} \tag{3.19}$$

In this analysis, two different predefined element types were utilized. PLANE77 and PLANE82 are among elements designed in ANSYS [37] that are used in this analysis. PLANE77 is a high order 2D, 4-node thermal element. Temperature is the only degree of freedom in this element. An 8-node element of PLANE77 is more suitable for curved boundaries and has compatible temperature shapes. By merging 3 nodes of this element 6-node triangular element can be achieved. PLANE82 similarly is a high order 2D, 4-node element. The most important properties of this element are accuracy when using quadrilateral and triangular elements simultaneously, compatible displacement shapes, and suitability of 8-node version for curved boundariesfigure-3.2 [37].

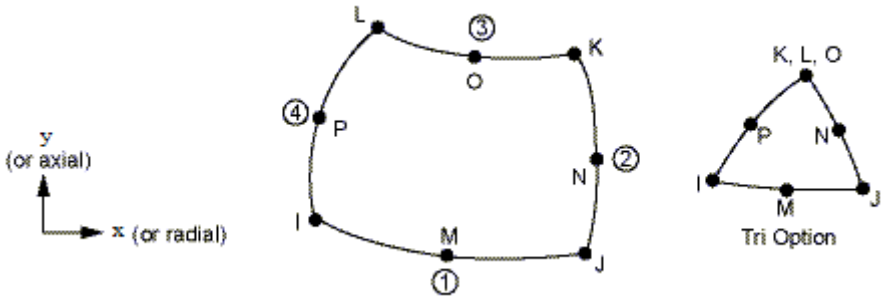

Figure 3.2: PLANE77 and PLANE82 elements and triangular versions

For both types of elements shape functions used for approximation are (APPENDIX C):

$$\psi_1 = -\frac{1}{4}(1-\xi)(1-\eta)(1+\xi+\eta) \tag{3.20a}$$

$$\psi_2 = \frac{1}{2}(1-\xi^2)(1-\eta) \tag{3.20b}$$

$$\psi_3 = -\frac{1}{4}(1+\xi)(1-\eta)(1-\xi+\eta) \tag{3.20c}$$

$$\psi_4 = \frac{1}{2}(1-\xi)(1-\eta^2) \tag{3.20d}$$

$$\psi_5 = \frac{1}{2}(1+\xi)(1-\eta^2) \tag{3.20e}$$

$$\psi_6 = -\frac{1}{4}(1-\xi)(1+\eta)(1+\xi-\eta) \tag{3.20f}$$

$$\psi_7 = -\frac{1}{4}(1-\xi^2)(1+\eta) \tag{3.20g}$$

$$\psi_8 = -\frac{1}{4}(1+\xi)(1+\eta)(1-\xi-\eta) \tag{3.20h}$$

In finite element implementation of the problem 8 node quadrilateral element is used for analysis of the model in all thermal, hygroscopic and structural analysis, but merging 3 nodes of the element 6 node triangular elements were produced, thus meshing of the model near the crack tip was better and easier, on the other hand use of interpolation functions of 8 node element provided more accurate results. Figure-3.1 illustrates the merging of nodes and global and isoparametric systems in element [25].

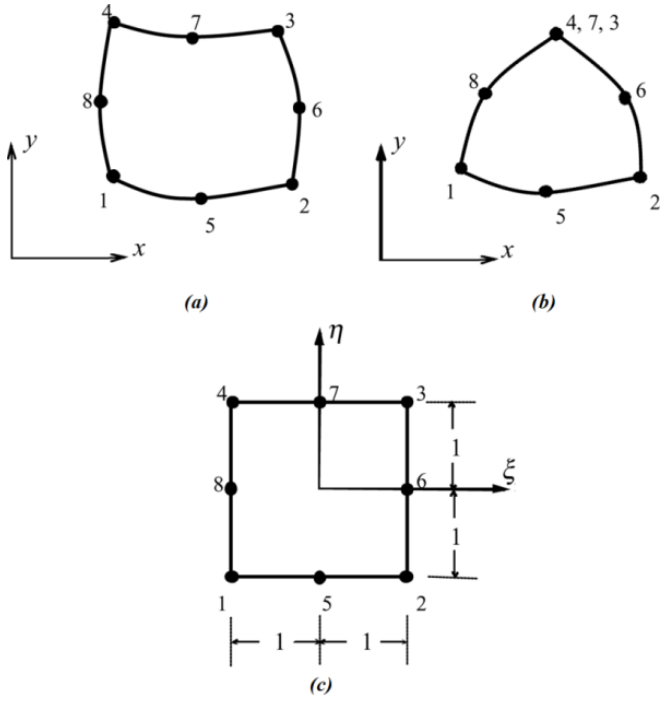

Figure 3.3: Illustration of an (a) eight node quadrilateral and a (b) six node triangular element both in global coordination system and (c) transformation of quadrilateral one in isoparametric coordination system

From Eq.(2.3.49), Eq.(2.4.1) and Eq.(2.4.2) it can be concluded that:

$$\widetilde{J_2} = \iint_A (\sigma_{ij} u_{i,2} - W\delta_{2j}) q_{,j} dA - \iint_A (W_{,2})_{expl} q dA - \int_0^{R-d} (W^+ - W^-) q ds \quad (i,j = 1,2) \tag{3.21}$$

As mentioned before line integrals in Eq.(3.21) are solved using Gauss-Legendre Quadrature (see APPANDIX C for the details). The components of line integral which are mechanical strain energy density and q , are computed previously determined in Eq.(2.3.4) and Eq.(2.3.28). Here and example of how line integrals are calculated is covered. The integral is for upper crack face and ond_1:

$$L_1 = \int_0^{R-d_1} W^+ q \, dx \tag{3.22}$$

Approximation using polynomial and also transformation to (ξ, η) coordination system will lead to:

$$L_1 \approx \sum_{i=1}^{2} W_i^+ \left(\frac{R - |x(\xi_i)|}{R}\right) |J| \tag{3.23}$$

The determinant of Jacobian can be determined using Eq.(3.16).

If we assume that the domain integral part of $\widetilde{J_2}$ to be $\widetilde{J_2}'$ then:

$$\widetilde{J_2}' = \sum_{k=1}^{2} \sum_{l=1}^{2} \widetilde{J_2}'' (\xi_k, \eta_l) \tag{3.24}$$

Eq.(3.21) requires calculation of stress which are found using strains and constitutive relations Eq.(2.2.1). Strains are found using displacements:

$$\varepsilon_{11} = \frac{\partial u_1}{\partial x_1} = \sum_{i=1}^{8} \frac{\partial \psi_i}{\partial x_1} u_{1i} \tag{3.25}$$

$$\frac{\partial u_1}{\partial x_2} = \sum_{i=1}^{8} \frac{\partial \psi_i}{\partial x_2} u_{1i} \tag{3.26}$$

$$\frac{\partial u_2}{\partial x_1} = \sum_{i=1}^{8} \frac{\partial \psi_i}{\partial x_1} u_{2i} \tag{3.27}$$

$$\varepsilon_{22} = \frac{\partial u_2}{\partial x_2} = \sum_{i=1}^{8} \frac{\partial \psi_i}{\partial x_2} u_{2i} \tag{3.28}$$

$$\varepsilon_{12} = \frac{1}{2}\left(\sum_{i=1}^{8} \frac{\partial \psi_i}{\partial x_2} u_{1i} + \sum_{i=1}^{8} \frac{\partial \psi_i}{\partial x_1} u_{2i}\right) \tag{3.29}$$

Finding mechanical strain energy function is one of the essentialities of the procedure. This term can be achieved by using Eq.(2.3.4), since it can be written in terms of strains.

The next mission is to find mechanical strain energy density function derivatives $\left(W_{,2}\right)_{expl}$. This step involves calculation of following terms:

$$\frac{\partial W}{\partial E_1}, \frac{\partial W}{\partial E_2}, \frac{\partial W}{\partial \nu_{12}}, \frac{\partial W}{\partial G_{12}}, \frac{\partial W}{\partial \alpha_1}, \frac{\partial W}{\partial \alpha_2}, \frac{\partial W}{\partial (\Delta T)}, \frac{\partial W}{\partial (\Delta c)} \tag{3.30}$$

$$\frac{\partial E_1}{\partial x_2}, \frac{\partial E_2}{\partial x_2}, \frac{\partial \nu_{12}}{\partial x_2}, \frac{\partial G_{12}}{\partial x_2}, \frac{\partial \alpha_1}{\partial x_2}, \frac{\partial \alpha_2}{\partial x_2}, \frac{\partial (\Delta T)}{\partial x_2}, \frac{\partial (\Delta c)}{\partial x_2} \tag{3.31}$$

These derivatives are calculated and presented in APPENDIX B.

Numerical calculation of these derivatives is lead on these formulations:

$$\frac{\partial E_1}{\partial x_2} = \sum_{i=1}^{8} \frac{\partial \psi_i}{\partial x_2} E_{1i} \tag{3.32}$$

$$\frac{\partial E_2}{\partial x_2} = \sum_{i=1}^{8} \frac{\partial \psi_i}{\partial x_2} E_{2i} \tag{3.33}$$

$$\frac{\partial \nu_{12}}{\partial x_2} = \sum_{i=1}^{8} \frac{\partial \psi_i}{\partial x_2} \nu_{12i} \tag{3.34}$$

$$\frac{\partial G_{12}}{\partial x_2} = \sum_{i=1}^{8} \frac{\partial \psi_i}{\partial x_2} G_{12i} \tag{3.35}$$

$$\frac{\partial \alpha_1}{\partial x_2} = \sum_{i=1}^{8} \frac{\partial \psi_i}{\partial x_2} \alpha_{1i} \tag{3.36}$$

$$\frac{\partial \alpha_2}{\partial x_2} = \sum_{i=1}^{8} \frac{\partial \psi_i}{\partial x_2} \alpha_{2i} \tag{3.37}$$

$$\frac{\partial (\Delta T)}{\partial x_2} = \sum_{i=1}^{8} \frac{\partial \psi_i}{\partial x_2} (\Delta T)_i \tag{3.38}$$

$$\frac{\partial(\Delta c)}{\partial x_2} = \sum_{i=1}^{8} \frac{\partial \psi_i}{\partial x_2} (\Delta c)_i \tag{3.39}$$

The derivatives of q needed in this calculation are:

$$q_{,1} = -\frac{x_1}{R\sqrt{x_1^2 + x_2^2}} \tag{3.40}$$

$$q_{,2} = -\frac{x_2}{R\sqrt{x_1^2 + x_2^2}} \tag{3.41}$$

Now remained terms that should be calculated are derivatives of shape functions with respect to global coordination system.

$$\frac{\partial \psi_i}{\partial \eta} = \frac{\partial \psi_i}{\partial x_1}\frac{\partial x_1}{\partial \eta} + \frac{\partial \psi_i}{\partial x_2}\frac{\partial x_2}{\partial \eta} \tag{3.42}$$

$$\frac{\partial \psi_i}{\partial \xi} = \frac{\partial \psi_i}{\partial x_1}\frac{\partial x_1}{\partial \xi} + \frac{\partial \psi_i}{\partial x_2}\frac{\partial x_2}{\partial \xi} \tag{3.43}$$

$$\begin{bmatrix} \frac{\partial \psi_i}{\partial x_1} \\ \frac{\partial \psi_i}{\partial x_2} \end{bmatrix} = \frac{1}{|J|} \begin{bmatrix} \frac{\partial x_2}{\partial \xi} & -\frac{\partial x_2}{\partial \eta} \\ -\frac{\partial x_1}{\partial \xi} & \frac{\partial x_1}{\partial \eta} \end{bmatrix} \begin{bmatrix} \frac{\partial \psi_i}{\partial \eta} \\ \frac{\partial \psi_i}{\partial \xi} \end{bmatrix} \tag{3.44}$$

J_1 can be calculated found the same way as $\widetilde{J_2}'$.

J_k-integral is calculated over circular domains with various diameters, but the main factors affecting the accuracy of the results are mesh density and the size of d shown in Eq.(2.4.1) and Eq.(2.4.2). Higher mesh density results relatively better outcomes, but process of a dense mesh would take more time, so an optimization was essential during mesh process. In order to fulfill both accuracy and efficiency of the model analysis, approximately 10^5 elements were generated and around crack tip and within integration boundaries density of meshes were designed to be higher, as shown in figure-3.2. During analysis process it was clear that a value of $(10^{-4})a$ for d_1 and $2(10^{-4})a$ for d_2 gives out an accurate result, so these values were given to d_1 and d_2 during analysis.

CHAPTER 4

NUMERICAL EXAMPLE AND RESULTS

4.1. Problem description

For hygrothermal fracture analysis of the orthotropic composite, a crack was embedded in the fiber reinforced composite as illustrated in figure-4.1.1. x_1 and x_2 are two principal axes of the sheet, and fiber volume was assumed to change along X_2 axes of the medium. V_{f_0} and V_{f_w} are minimum and maximum fiber volumes in the composite sheet respectively. The extremums of the volume were considered to be at the lower and upper boundaries of the medium. Boundary conditions for the problem are illustrated in figure-4.1.2, C and T resemble respectively hygroscopic and thermal boundary conditions. The problem is solved for cracks embedded in different locations of the composite sheet, 0.1, 0.2, 0.3 and 0.4 were taken as the value of h_1; consequently four different models were simulated and analyzed. Volume of the fiber is designed to be a function of X_2 and also P, as it can be seen obviously from Eq.(4.1.1) V_{f_0} , and took values equal to 0.1, 0.2, 0.3 and 0.4, and V_{f_w} had the value of 0.7 through calculations. In Eq.(4.1.1), P as an exponent defines the properties of the sheet, so by changing P from 0 to infinity during calculations, solution will be done for several models. Considering both physical and material models, solutions were done for 256 different mediums.

$$V_f(x_2) = V_{f_0} + \left(V_{f_w} - V_{f_0}\right).\left(\frac{x_2}{h}\right)^p \tag{4.1.1}$$

$$V_m(x_2) = 1 - V_f(x_2) \tag{4.1.2}$$

In the equations above V_f stands for volume of the fiber and V_m stands for volume of the matrix.

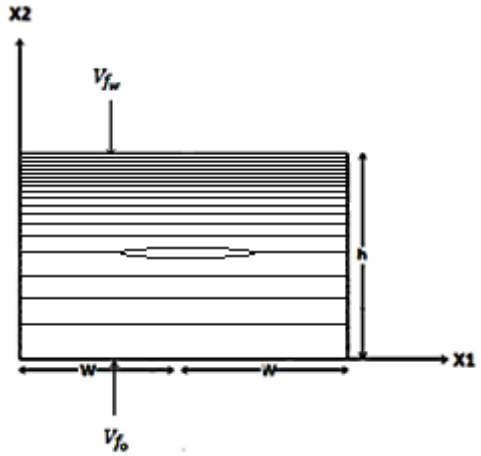

Figure 4.1.1: Crack embedded in fibrous composite with variable fiber spacing

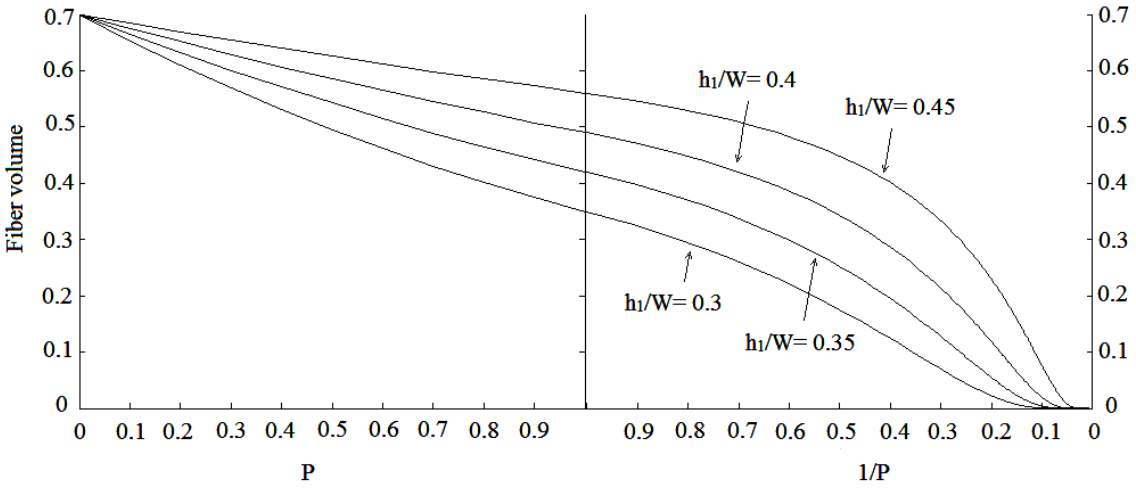

Figure 4.1.2: Fiber volume at crack tip for different crack locations

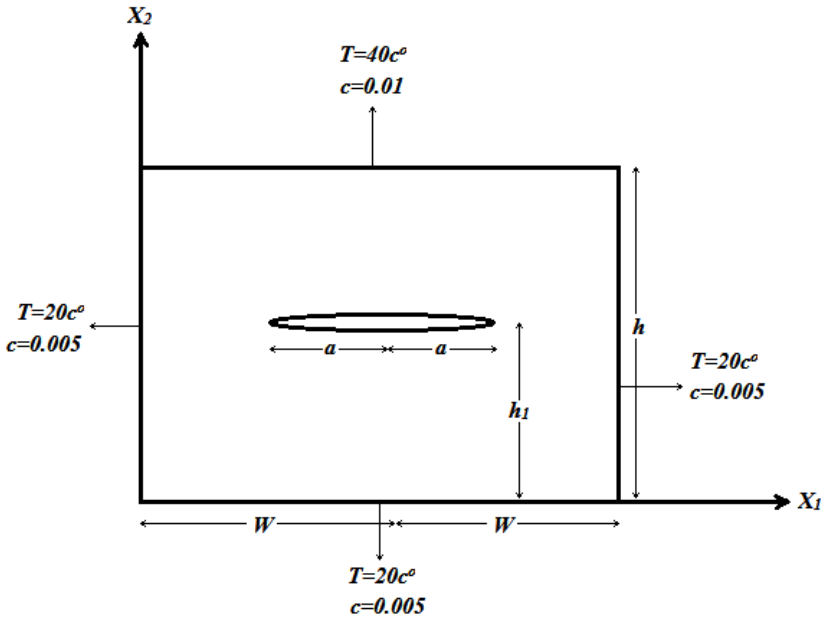

(b)

Figure 4.1.3: Boundary conditions for the problem

Mechanical properties of the fibrous composites are defined as:

$$E_1(x_2) = E_f V_f(x_2) + E_m V_m(x_2), \qquad \frac{1}{E_2(x_2)} = \frac{V_f(x_2)}{E_f} + \frac{V_m(x_2)}{E_m} \tag{4.1.2a}$$

$$\frac{1}{G_{12}(x_2)} = \frac{V_f(x_2)}{G_f} + \frac{V_m(x_2)}{G_m}, \qquad \nu_{12}(x_2) = \nu_f V_f(x_2) + \nu_m V_m(x_2) \tag{4.1.2b}$$

$$\alpha_1(x_2) = \frac{1}{E_1(x_2)}\left(\alpha_f E_f V_f(x_2) + \alpha_m E_m V_m(x_2)\right),$$
$$\alpha_2(x_2) = \left(1 + v_f\right)\alpha_f V_f(x_2) + (1 + v_m)\alpha_m V_m(x_2) - \alpha_1(x_2)v_{12} \tag{4.1.2c}$$

$$\beta_1(x_2) = \frac{E_m}{E_1(x_2)}\frac{\left(\rho_f V_f(x_2) + \rho_m V_m(x_2)\right)}{\rho_m}\beta_m$$
$$\beta_2(x_2) = (1 + v_m)\frac{\rho_f V_f(x_2) + \rho_m V_m(x_2)}{\rho_m}\beta_m \tag{4.1.2d}$$

$$k_1(x_2) = k_f V_f(x_2) + k_m V_m(x_2)$$
$$k_2(x_2) = \frac{1 + \eta V_f(x_2)}{1 - \eta V_f(x_2)}k_m, \qquad \eta = \frac{\frac{k_f}{k_m} - 1}{\frac{k_f}{k_m} + 1} \tag{4.1.2e}$$

$$D_1(x_2) = D_m V_m(x_2), \qquad D_2(x_2) = \left(1 - 2\sqrt{\frac{V_f(x_2)}{\pi}}\right)D_m \tag{4.1.2f}$$

In the equations above, m and f stand for matrix and fiber property in the sheet respectively.

The solution of the problem is achieved by finding the solution for the half of the actual medium, since the medium is symmetric in x_1 direction.Thus simulating a half model with an insulated boundary condition in the cut face, would give us the desired solution figure-4.1.4. So the whole process during simulation and solution is carried out for crack at $x_1 = a$, but after finding crack parameters at this crack tip we can find the parameters for the other one as shown below:

$$J_1(-a) = J_1(a), \qquad J_2(-a) = J_2(a) \tag{4.1.3a}$$

$$K_I(-a) = K_I(a), \qquad K_{II}(-a) = -K_{II}(a) \tag{4.1.3b}$$

$$T_s(-a) = T_s(a) \tag{4.1.3c}$$

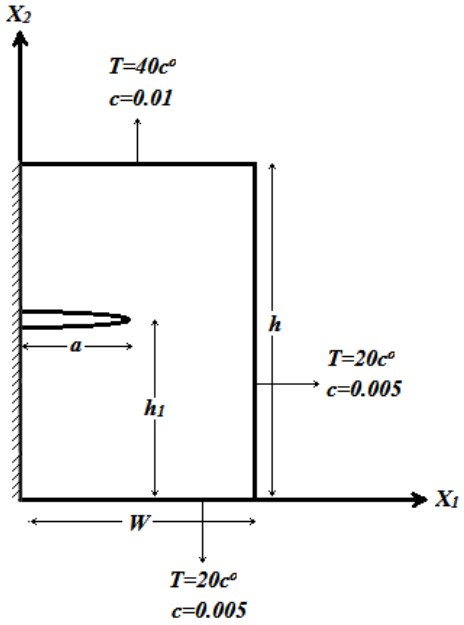

Figure 4.1.4: Simulated medium and the boundary conditions

4.2. Hygrothermal superposition in the results

As mentioned before, according to Eq.(2.1.1) the relation between thermal and hygroscopic part of the constitutive equation is linear, and in section 2.2 from comprehensive expressions of the formulation and also derivatives presented in APPANDIX B we can clearly infer linearity of the relation between thermal and hygroscopic part. This admits the validity of superposition method in finding hygrothermal results, which is simply adding up SIF found in hygroscopic analysis and SIF found in thermal analysis and achieving hygrothermal stress intensity factor as shown in Eq.(4.2.1).

$$K_I = K_I^{Thermal} + K_I^{Hygroscopic} \tag{4.2.1}$$

$$K_{II} = K_{II}^{Thermal} + K_{II}^{Hygroscopic} \tag{4.2.2}$$

$$T_s = T_s^{Thermal} + T_s^{Hygroscopic} \tag{4.2.3}$$

J_2 is the energy release rate and it's defined in terms of K_I and K_{II}, so it can be hygroscopic and thermal result can be superposed by the means of using superposed K_I and K_{II} in the formulation. This is the superposition algorithm of the APDL code. In the following section tables showing both comparison of the results with DCT technique and also the superposition of the results are presented.

4.3. Validation for the results and comparison with DCT technique

As previously presented in figure figure-4.1.1 and figure-4.1.2, a fibrous composite sheet with variable spaced fiber and a crack with length of $2a$ is embedded in different locations of the plate in

various analysis. $T_r = T_0$ is defined as reference temperature and as shown in figure-4.1.2, temperature at boundary of $X_2 = h$ is equal to $2T_0$, and on the other boundaries it is equal to T_0. Since the analysis was hygrothermal, hygroscopic boundary conditions had to be defined too. $c_r = 0$ is defined as the reference moisture concentration value in the plate, and for the boundary at $X_2 = h$, moisture concentration is equal to $2c_0$ and at other boundaries it is equal to c_0. The crack faces are assumed to be insulated both for thermal and hygroscopic case, and that means no thermal flux and moisture concentration flux is provided at these faces. Considering all the analysis in this paper, most of the variables are changing in different models, but for all the models $T_0, c_0, h \; and \; W$ remain the same and equal to $T_0 = 20$, $c_0 = 0.005$, $h = 2.5$ and $W = 5$.

In Eq.(4.1.2),m and f in the variables show the relation of the property with matrix and fiber material respectively. α shows the thermal expansion ratio and β represents moisture expansion ratio. Matrix is chosen to be epoxy and fibers in the matrix are glass fiber. Properties for these materials are presented in Table-4.3.1.

Table 4.3.1: Material properties for matrix and fiber

	Epoxy matrix	**Glass Fiber**
E(Gpa)	3.4	85
G(Gpa)	1.308	35.42
ν	0.3	0.2
α(1/^{0}C)	63(10)$^{-6}$	5(10)$^{-6}$
β	0.33	N/A
ρ(Kg/m^3)	1200	2500
k(W/m^{0}C)	0.25	1.05
D(m^2/s)	3(10)$^{-15}$	N/A

Calculations are carried out using different domain circles, the domain independency of J_k-integral is proven using outcomes of solutions for different domains; however a validation for the results gained using J_k-integral is needed. For this purpose, table 4.3.2-4.3.4 are prepared to show both the results achieved using J_k-integral and results for the same model achieved using another method called displacement correlation technique (DCT) [28, 29].

For presentation of the results some kind of normalization of the data was required, thus in all the results Eq.(4.3.1) was used to make result normalized.

$$K_{In} = \frac{K_I}{\alpha_m E_m T_0 \sqrt{\pi a}} \tag{4.3.1a}$$

$$K_{IIn} = \frac{K_{II}}{\alpha_m E_m T_0 \sqrt{\pi a}} \tag{4.3.1b}$$

$$J_{In} = \frac{J_I}{E_m \alpha_m^2 T_0^2 \pi a} \tag{4.3.1c}$$

$$T_{sn} = \frac{T_s}{\alpha_m E_m T_0} \tag{4.3.1d}$$

In the following figures, deformation of the model under effect of thermal and hygroscopic loads is illustrated. In figure-4.3.1, distribution of temperature and moisture concentration can be observed over the medium and especially around crack tip and boundaries. In figure-4.3.15 since the picture is related to the deformed shape, crack opening is visible, and it is absolutely clear that meshes are getting denser as we get closer to the crack tip.

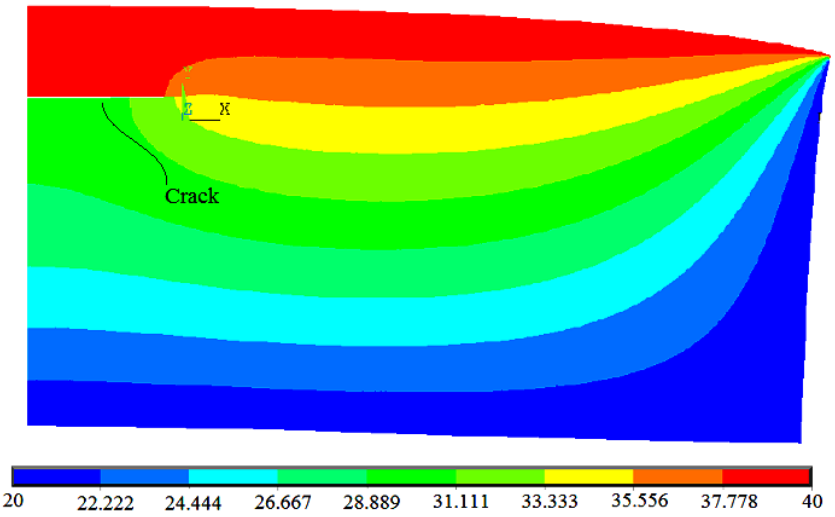

(a)

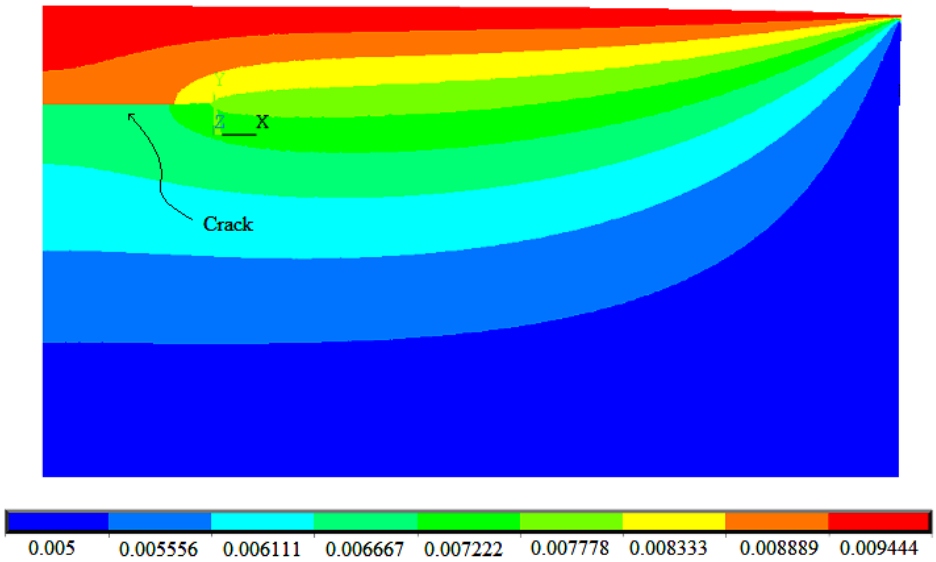

(b)

Figure 4.3.1: (a) Contour plot illustrating temperature distribution on the medium and structural deformation caused by thermal load (b) Contour plot illustrating moisture concentration distribution on the medium and structural deformation caused by hygroscopic load

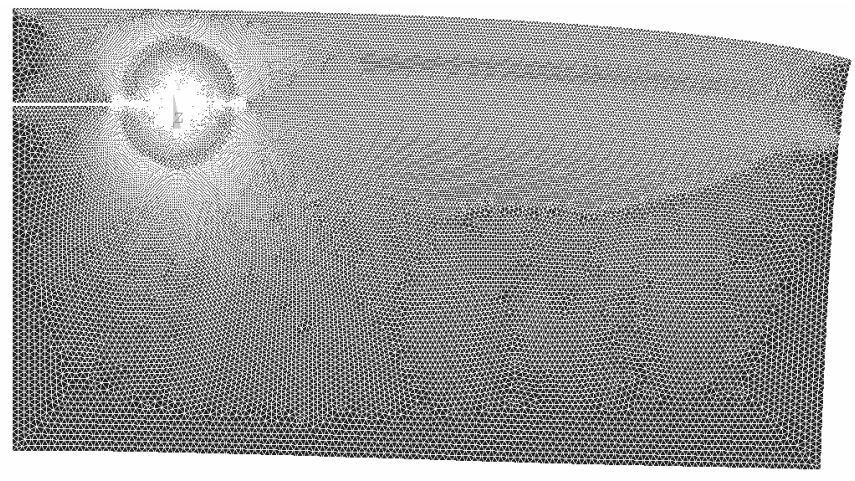

Figure 4.3.2: A scheme of meshing on the plate and deformation for h_1/w=0.4

In the following tables it can be observed that as mentioned before in section 4.2, two different tables are presented for two distinct boundary conditions. Table 4.3.2 shows results for thermal solution and Table 4.3.3 shows results for hygroscopic analysis. Superposition of these results is calculated using Eq.(4.2.1), Eq.(4.2.2) and Eq.(4.2.3) and shown in Table 4.3.4, to obtain hygrothermal analysis results of the model.

Table 4.3.2: Results of plain stress thermal solution for the model $w = 5,\ h = 2.5, h_1 = 2,\ a = 1,$ $V_{f_0} = 0.1, P = 0.1$

	DCT		**Jk-integral**	
R/a	KI	KII	KI	KII
0.1	0.02202	0.05662	0.02198	0.05707
0.2	0.02202	0.05662	0.02201	0.05705
0.3	0.02202	0.05662	0.02201	0.05704
0.4	0.02202	0.05662	0.02202	0.05704
Thermal				

Table 4.3.3: Results of plain stress Hygroscopic solution for the model $w = 5,\ h = 2.5,\ h_1 = 2,$ $a = 1, V_{f_0} = 0.1, P = 0.1$

	DCT		**Jk-integral**	
R/a	KI	KII	KI	KII
0.1	0.04218	0.09552	0.04203	0.09639
0.2	0.04218	0.09552	0.04216	0.09626
0.3	0.04218	0.09552	0.04225	0.09618
0.4	0.04218	0.09552	0.04229	0.09613
Hygroscopic				

Table 4.3.4: Results of plain stress Hygrothermal solution for the model $w = 5,\ h = 2.5,\ h_1 = 2,\ a = 1, V_{f_0} = 0.1, P = 0.1$

	DCT		Jk-integral		Percent difference	
R/a	KI	KII	KI	KII	KI	KII
0.1	0.064202	0.152135	0.06401	0.15346	0.29	0.86
0.2	0.064202	0.152135	0.06417	0.15331	0.05	0.76
0.3	0.064202	0.152135	0.06426	0.15322	0.09	0.71
0.4	0.064202	0.152135	0.06431	0.15317	0.17	0.67
Hygrothermal						

It is clear from the tables above that DCT and J_k-integral give out nearly the same results, which admits the validity of them. Last column in Table 4.3.4, shows the difference between results of two methods, and for the special case presented here it can be seen that all the results have <1% difference which proves the accuracy if the analysis carried out.

4.4. Result graphs for distinct material models

The graphs for the interpretation of the results for solution of the mediums with various dimensions and crack location, and also several values for the minimum and maximum fiber volume at the lower and upper boundaries are presented below.

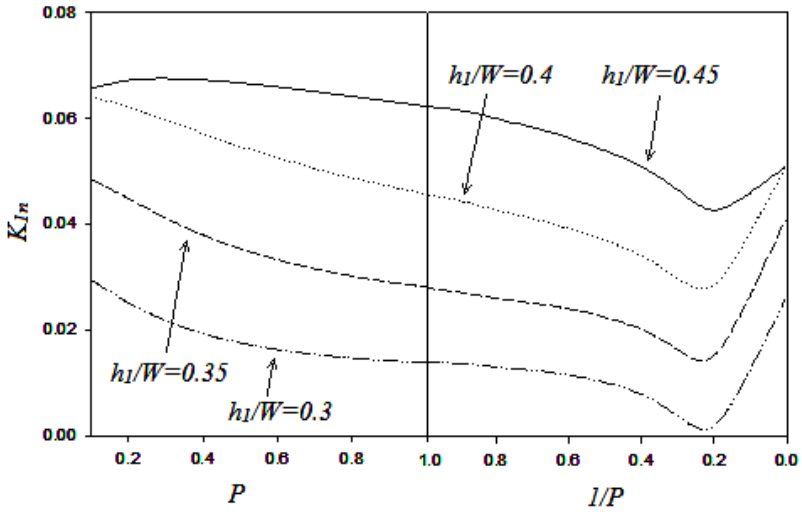

Figure 4.4.1: Normalized first mode SIF for the model $w = 5,\ h = 2.5,\ a = 1, V_{f_0} = 0.1$

As it can be observed in Figure-4.4.1, K_{In} decreases as P increases, but at a point around $1/P = 0.2$ there seems to be a critical point for the composite, in which it's behavior suddenly changes. This fact is also true for results presented in the following figures. It should be also mentioned that in all the results a distinction in behavior of the crack imbedded in $h_1/W = 0.45$ can be seen, which is slight tendency of its plot to the $h_1/W = 0.3$ case, so a careful look at these plots may lead to the inference, that there exists a point between $h_1/W = 0.4$ and $h_1/w = 0.45$, in which most of the parameters are at maximum value.

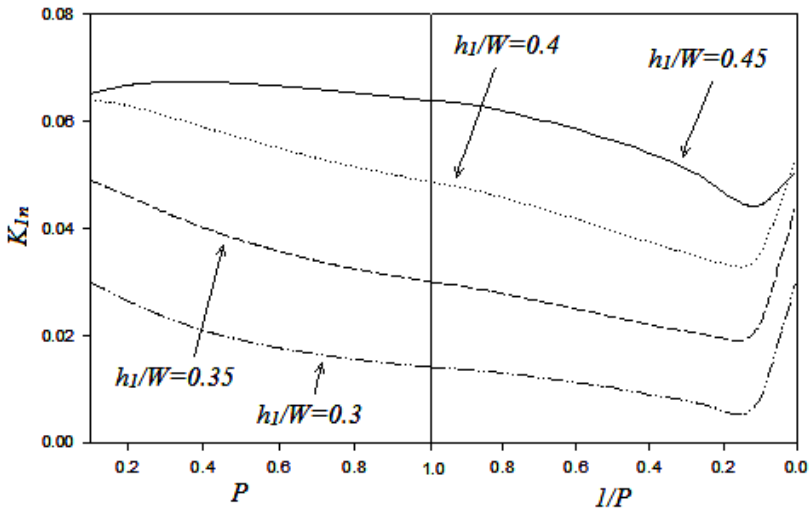

(a)

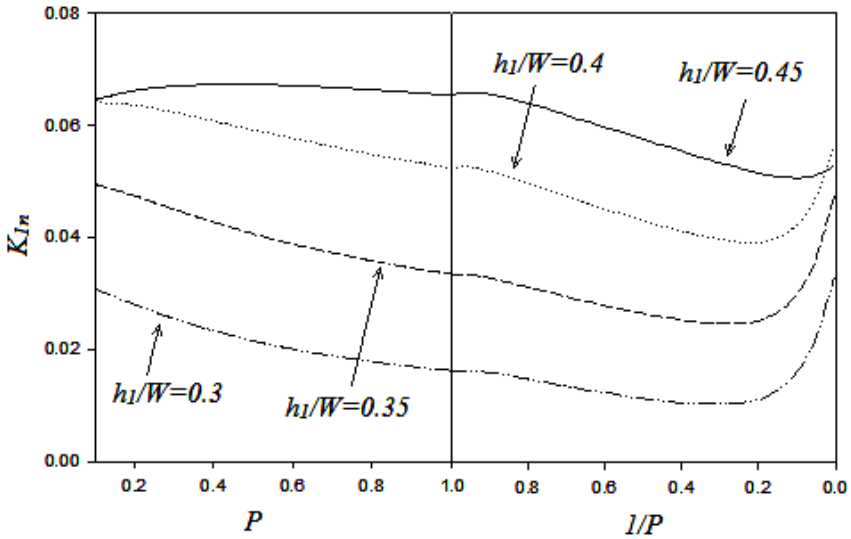

(b)

Figure 4.4.2: (a) Normalized first mode SIF for the model $w = 5$, $h = 2.5$, $a = 1$, $V_{f_0} = 0.2$ (b) Normalized first mode SIF for the model $w = 5$, $h = 2.5$, $a = 1$, $V_{f_0} = 0.3$

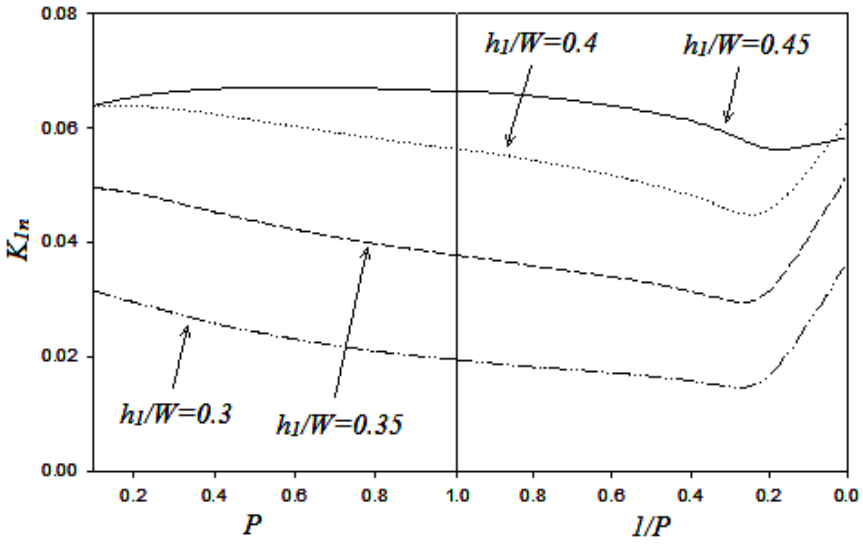

(a)

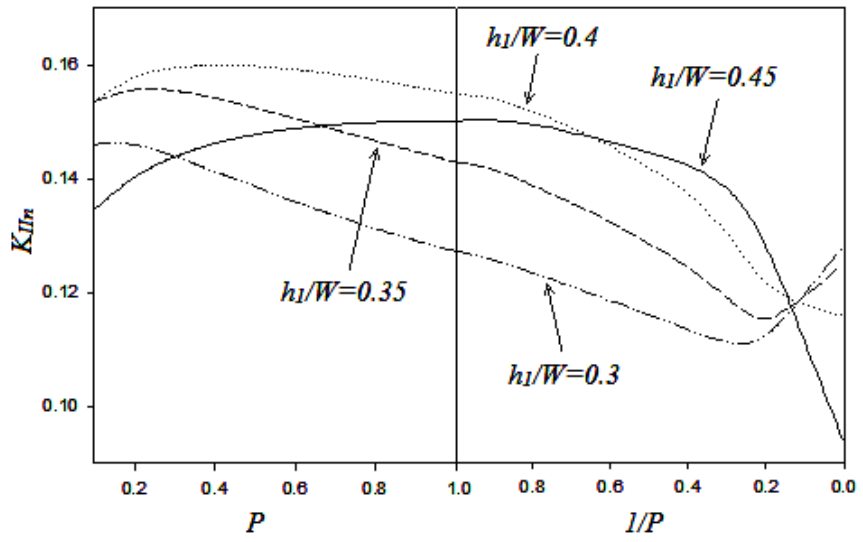

(b)

Figure 4.4.3:(a) Normalized first mode SIF for the model $w = 5$, $h = 2.5$, $a = 1$, $V_{f_0} = 0.4$
(b)Normalized second mode SIF for the model $w = 5$, $h = 2.5$, $a = 1$, $V_{f_0} = 0.1$

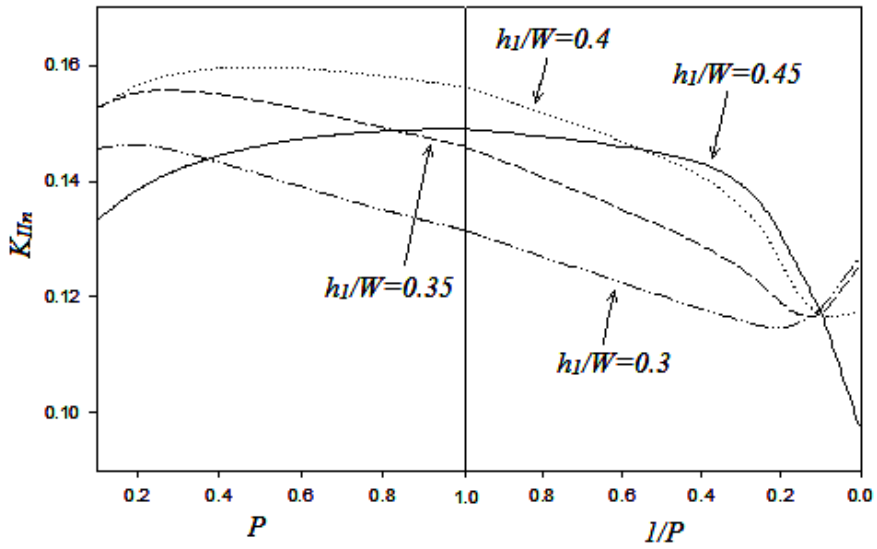

(a)

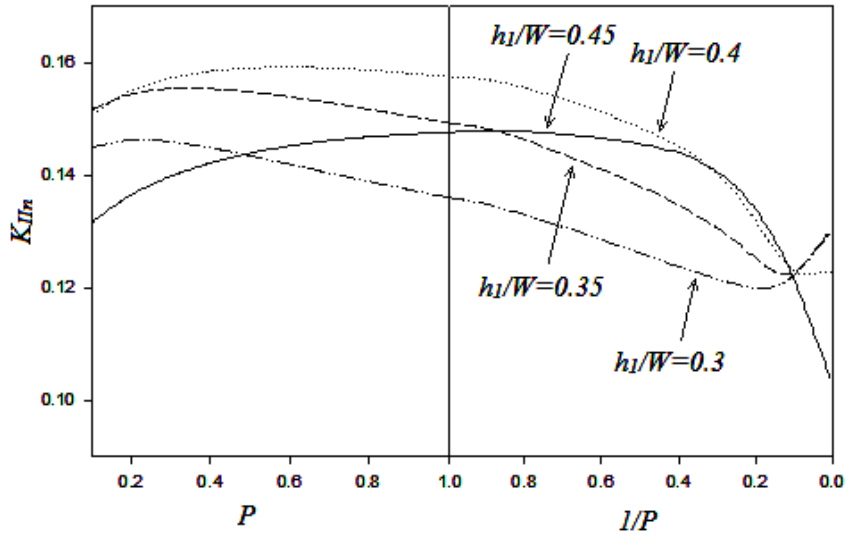

(b)

Figure 4.4.4: (a) Normalized second mode SIF for the model $w = 5$, $h = 2.5$, $a = 1$, $V_{f_0} = 0.2$ (b) Normalized second mode SIF for the model $w = 5$, $h = 2.5$, $a = 1$, $V_{f_0} = 0.3$

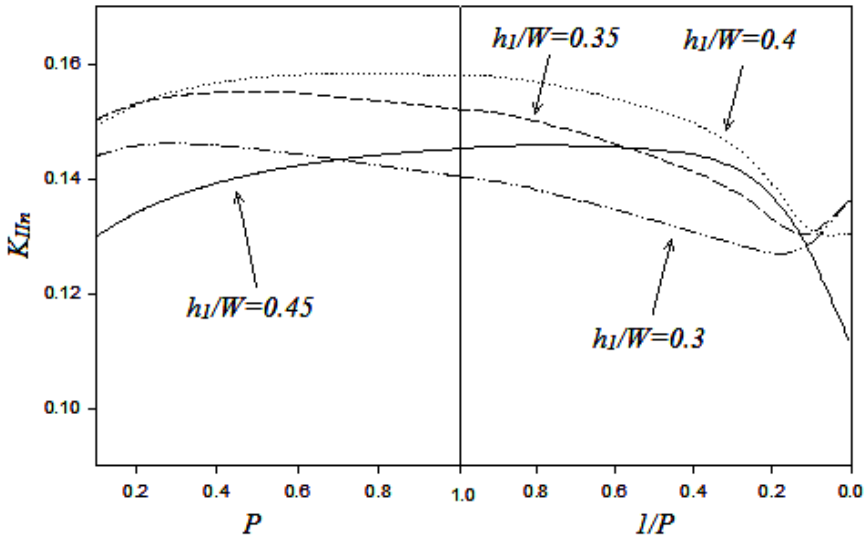

(a)

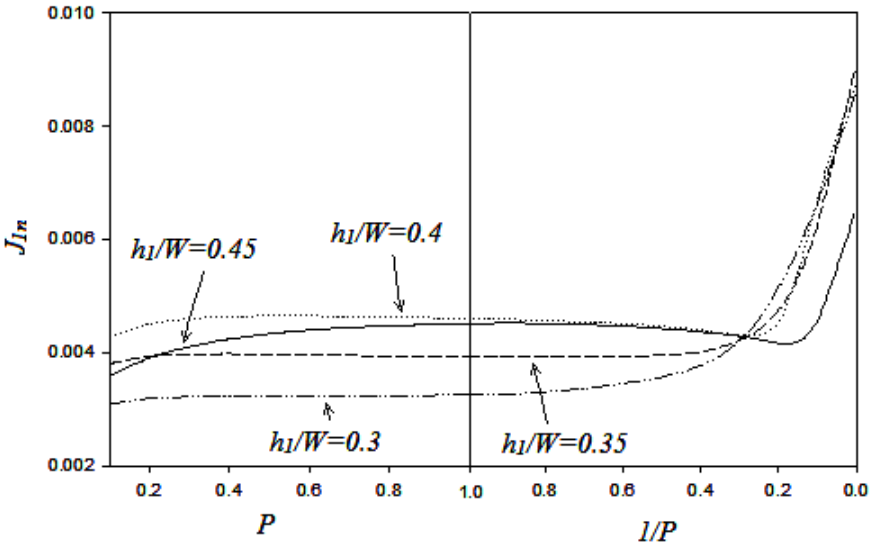

(b)

Figure 4.4.5: (a) Normalized second mode SIF for the model $w = 5$, $h = 2.5$, $a = 1$, $V_{f_0} = 0.4$ (b) Normalized energy release rate for the model $w = 5$, $h = 2.5$, $a = 1$, $V_{f_0} = 0.1$

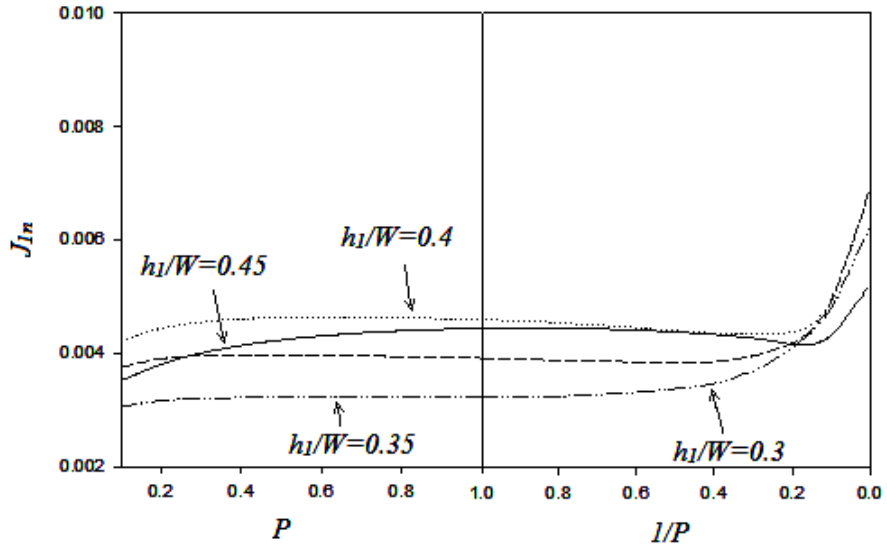

(a)

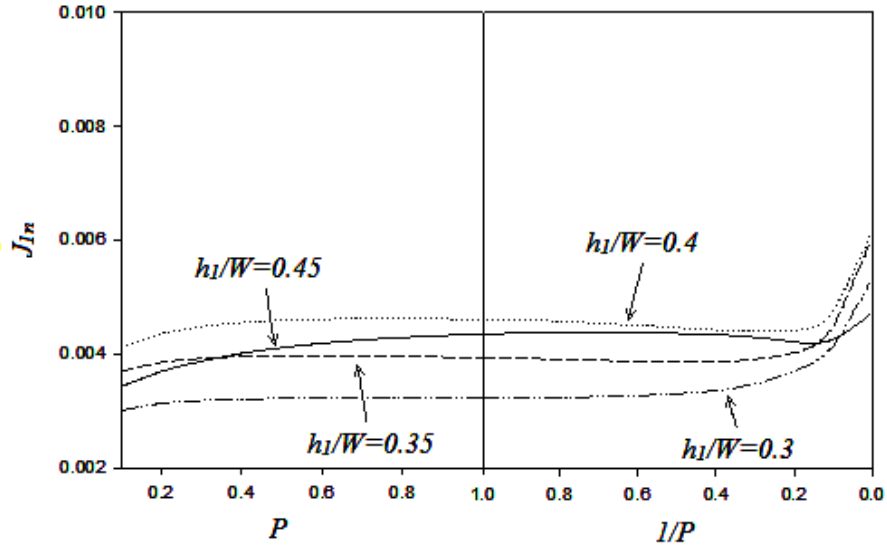

(b)

Figure 4.4.6: (a) Normalized energy release rate for the model $w = 5$, $h = 2.5$, $a = 1$, $V_{f_0} = 0.2$ (b) Normalized energy release rate for the model $w = 5$, $h = 2.5$, $a = 1$, $V_{f_0} = 0.3$

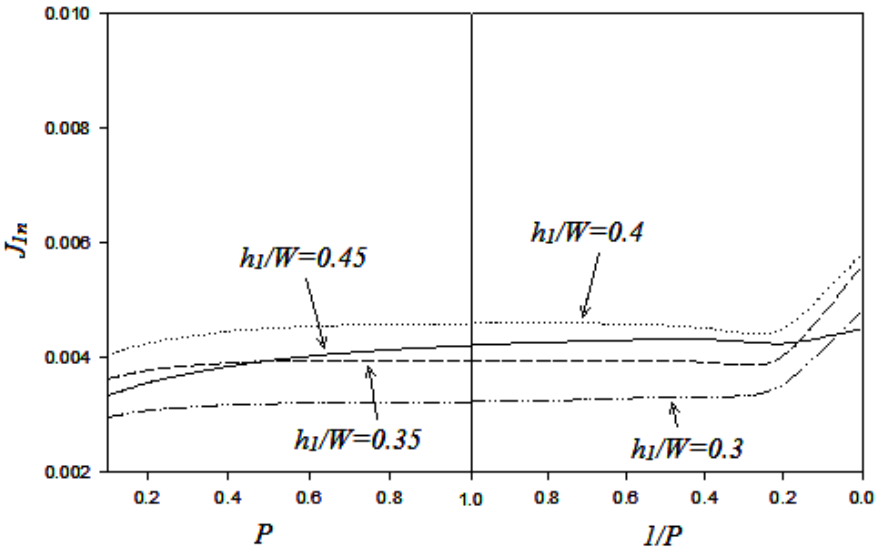

(a)

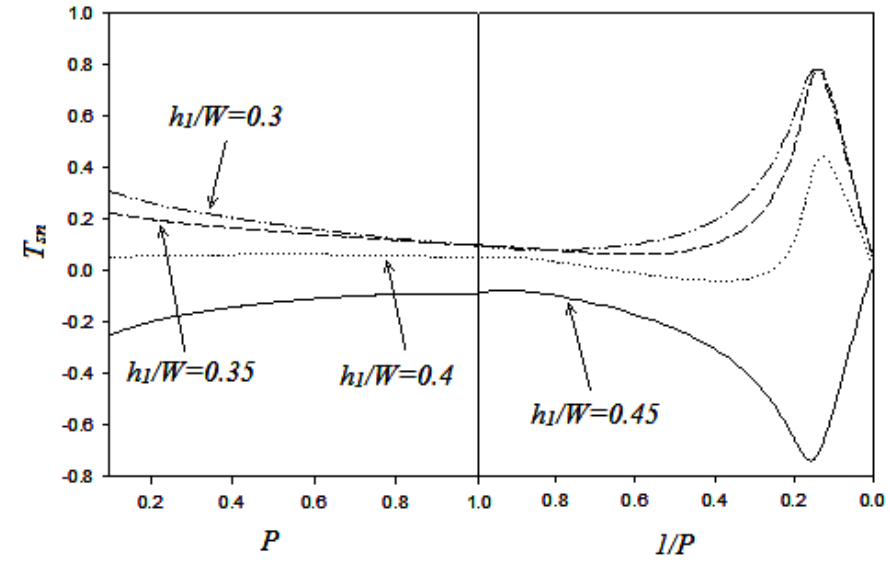

(b)

Figure 4.4.7: (a) Normalized energy release rate for the model $w = 5$, $h = 2.5$, $a = 1$, $V_{f_0} = 0.4$ (b) Normalized T-stress for the model $w = 5$, $h = 2.5$, $a = 1$, $V_{f_0} = 0.1$

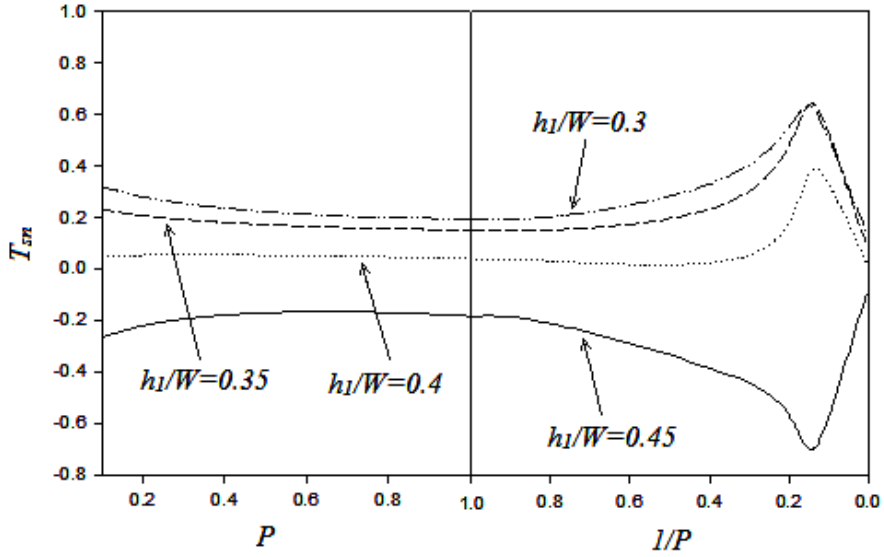

(a)

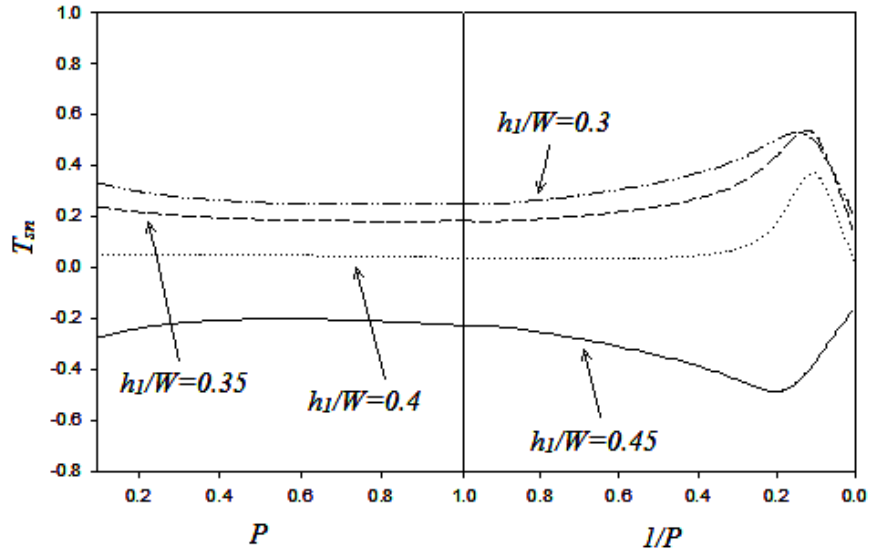

(b)

Figure 4.4.8: (a) Normalized T-stress for the model $w = 5$, $h = 2.5$, $a = 1$, $V_{f_0} = 0.2$

(b) Normalized T-stress for the model $w = 5$, $h = 2.5$, $a = 1$, $V_{f_0} = 0.3$

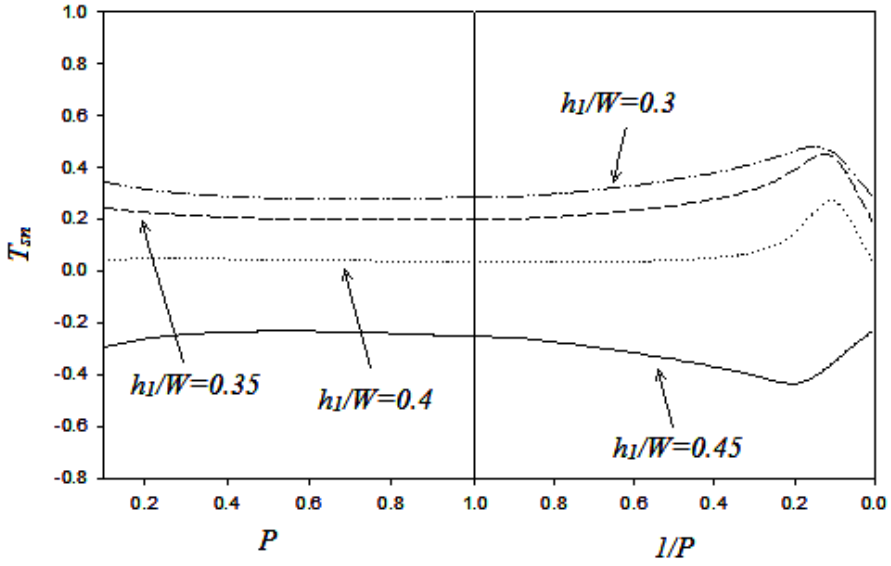

Figure 4.4.9: Normalized T-stress for the model $w = 5$, $h = 2.5$, $a = 1$, $V_{f_0} = 0.4$

4.5. Result graphs for models with crack length variation

In order to analyze the effect of the crack length on the fracture parameters of the crack, several mediums were modeled having crack lengths in the interval of $1 \leq a \leq 4$ .Plots showing the results for crack length variation are presented below. The boundary conditions for all the models are the same as previous analyzes. V_{f_0} is equal to 0.3 and in order to get a comprehensive understanding of effect of change in size of crack length on the results, solutions are found for P =0.5, P=0 and P=5, which means 3 different equations for fiber volume change through the sheet are taken into consideration.

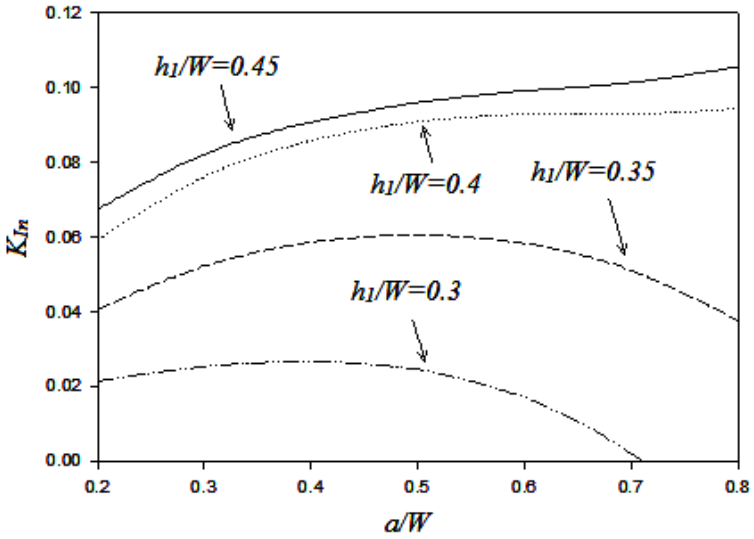

(a)

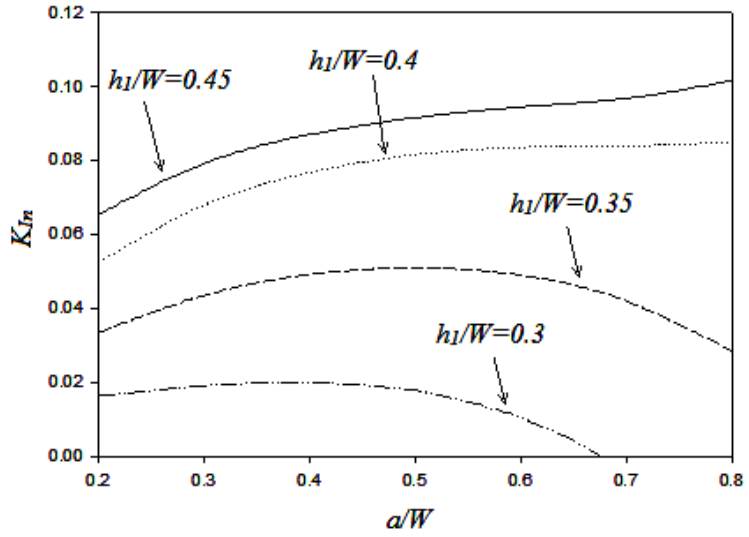

(b)

Figure 4.5.1: (a) Normalized first mode SIF for the model $w = 5$, $h = 2.5$, $V_{f_0} = 0.3$, $P = 0.5$ (b) Normalized first mode SIF for the model $w = 5$, $h = 2.5$, $V_{f_0} = 0.3$, $P = 1$

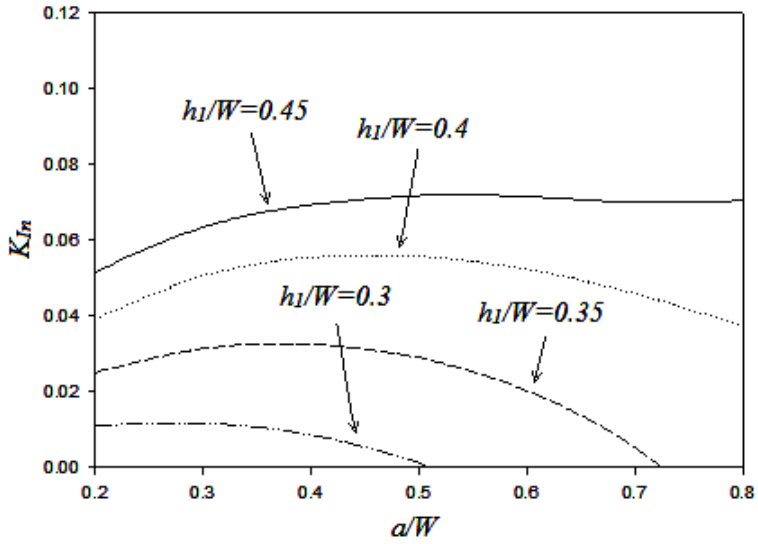

(a)

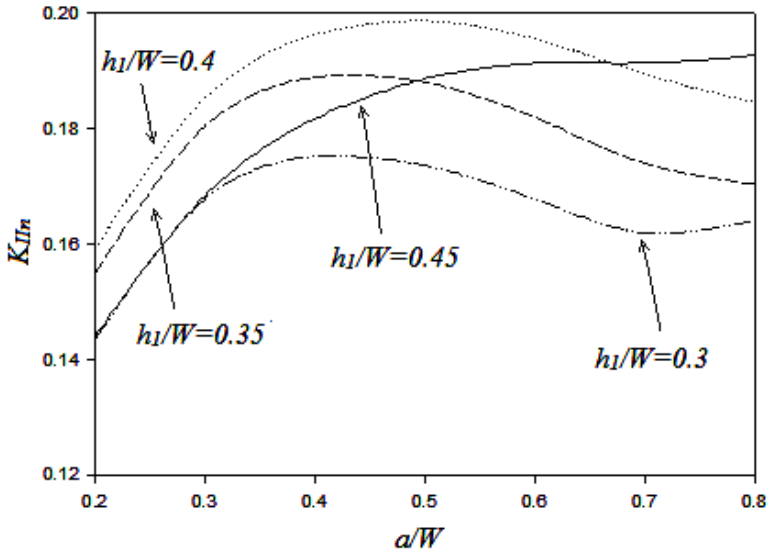

(b)

Figure 4.5.2: (a) Normalized first mode SIF for the model $w = 5$, $h = 2.5$, $V_{f_0} = 0.3$, $P = 5$ (b) Normalized second mode SIF for the model $w = 5$, $h = 2.5$, $V_{f_0} = 0.3$, $P = 0.5$

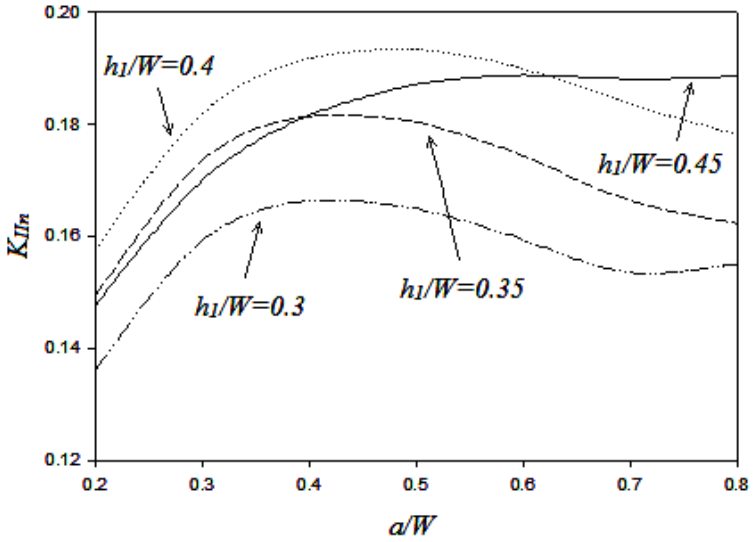

(a)

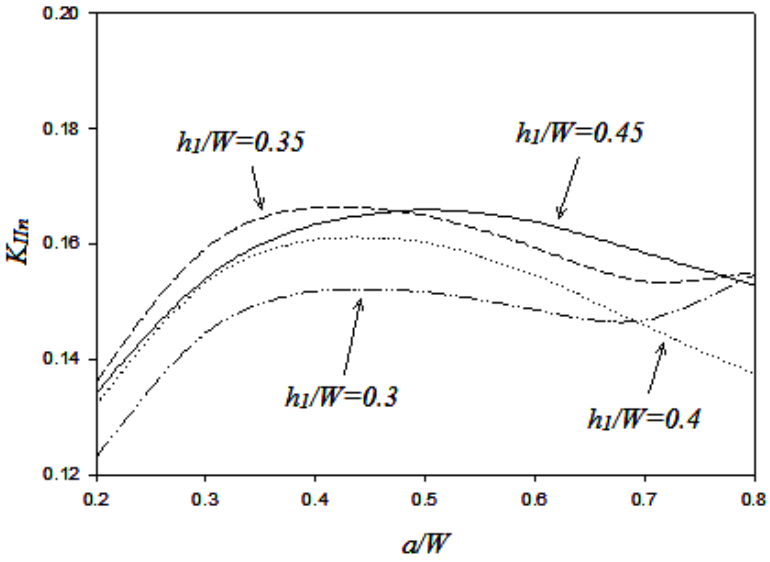

(b)

Figure 4.5.3: (a) Normalized second mode SIF for the model $w = 5$, $h = 2.5$, $V_{f_0} = 0.3$, $P = 1$ (b) Normalized second mode SIF for the model $w = 5$, $h = 2.5$, $V_{f_0} = 0.3$, $P = 5$

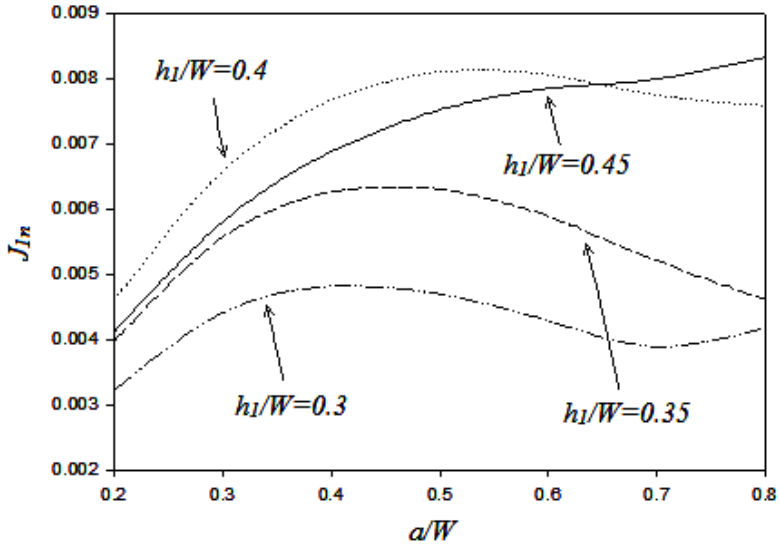

(a)

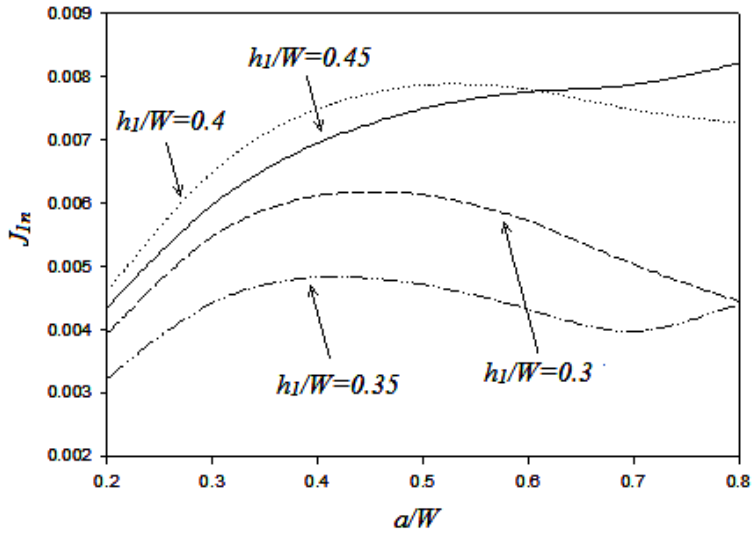

(b)

Figure 4.5.4: (a) Normalized energy release rate for the model $w = 5$, $h = 2.5$, $V_{f_0} = 0.3$, $P = 0.5$ (b) Normalized energy release rate for the model $w = 5$, $h = 2.5$, $V_{f_0} = 0.3$, $P = 1$

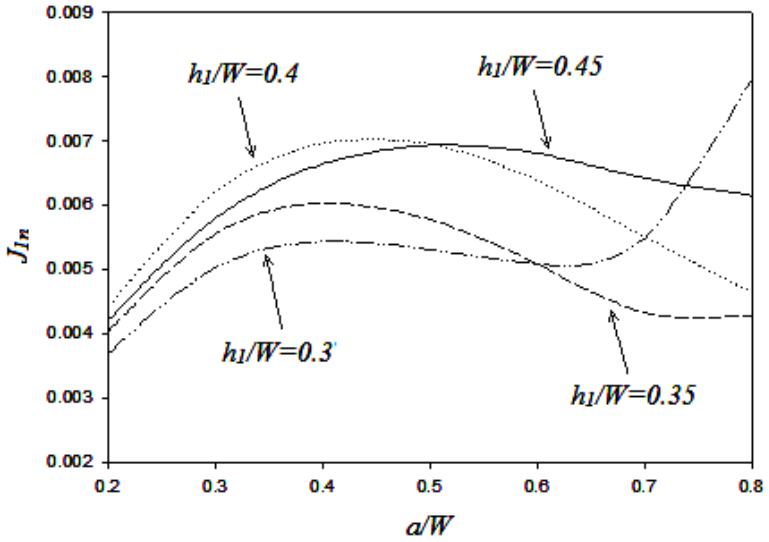

(a)

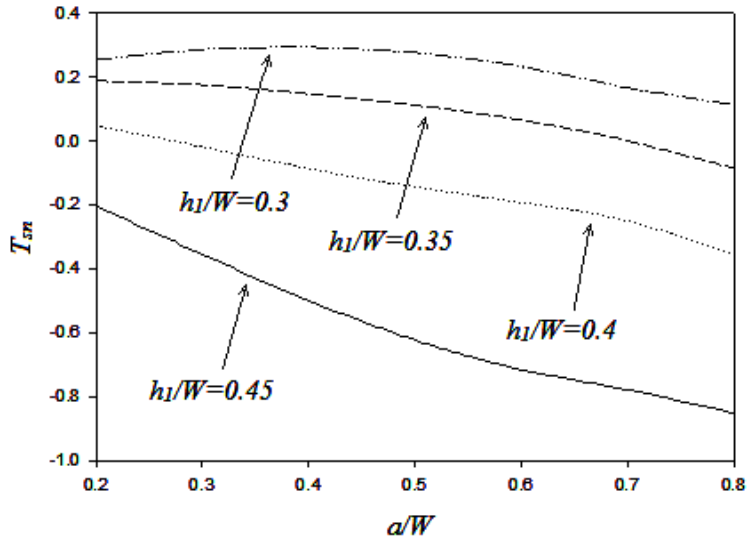

(b)

Figure 4.5.5: (a) Normalized energy release rate for the model $w = 5$, $h = 2.5$, $a = 1$, $V_{f_0} = 0.3$, $P = 5$ (b) Normalized T-stress for the model $w = 5$, $h = 2.5$, $a = 1$, $V_{f_0} = 0.3$, $P = 0.5$

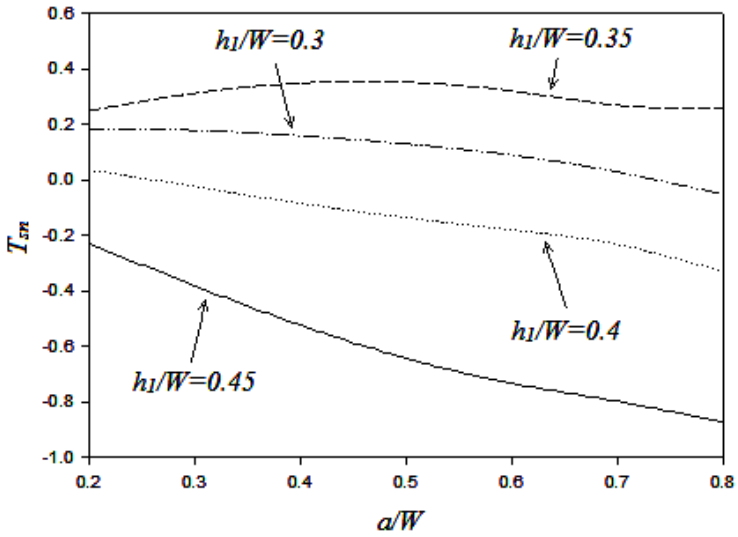

(a)

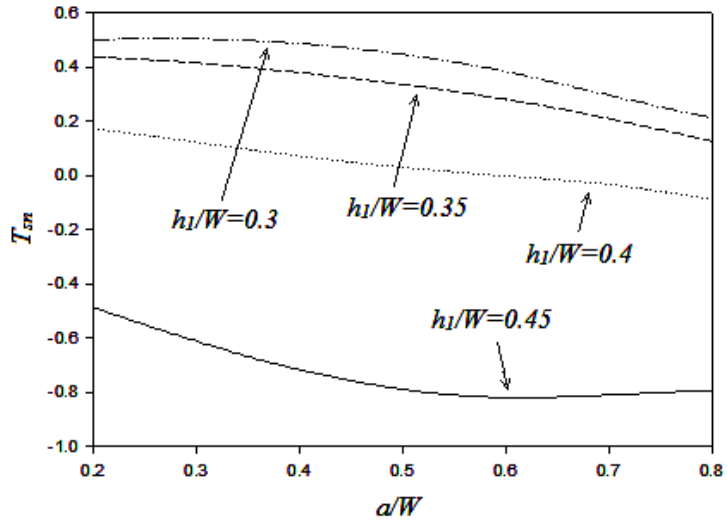

(b)

Figure 4.5.6: (a) Normalized T-stress for the model $w = 5$, $h = 2.5$, $a = 1$, $V_{f_0} = 0.3$, $P = 1$(b) Normalized T-stress for the model $w = 5$, $h = 2.5$, $a = 1$, $V_{f_0} = 0.3$, $P = 5$

CHAPTER 5

CONCLUTION

In this study, J_k-integral is manipulated as a new method to analyze fracture parameters of fiber reinforced composites with variable fiber spacing under hygrothermal boundary conditions. For this purpose, constitutive relations of plane orthotropic hygrothermoelasticity was used in formulation of J_k-integral, and providing a domain independency form for the formulation, during the computation procedure, definite technique was used to make J_k-integral formula accurately solvable by the means of finite element method. Chapter 4 includes several plots presenting fracture parameters as outcome of the analysis for model with different positions of crack and variety of crack lengths. Some pictures are also placed among results to show distribution of heat and moisture concentration separately in the medium during analysis. Also deformed shape of the model, crack opening and meshing system are among presented results for the solution.

Results indicate that generally crack propagation inhabitation is easily controllable in composites with variable spaced fibers, and comparison of the energy release rate in composites having the property $1/P$=0 (equally spaced fibers) with those having P equal to other values, reveals that composites with variable fiber spacing are behaving quite better than equally spaced ones in every aspect.

As mentioned before, one of the most outstanding properties of J_k-integral is giving out T-stress and energy release rate as result in addition to SIFs. T-stress is known as a critical factor as a crack parameter in analysis, which determines the crack kinking angle and also plastic zone size around crack tip. As a conclusion, investigation of T-stress would show accuracy of the results gained for the crack. It's totally clear from the results that the same explanations as energy release rate are not valid for T-stress outcomes of analysis, and functionally spaced fibers seem to have less accurate results than equally spaced ones in general, since in general, its magnitude is larger than T-stress value for FRC with variable fiber spacing.

The method used in this study gives a good understanding of how fibrous composites with variable fibers would behave subjected to hygrothermal loading. This technique can be extended to find crack parameters in functionally graded materials (FGMs) having functional mechanical properties changing with various functions and also composites having residual stresses induced by fabrication process.

REFERENCES

[1] **GIBSON, R.F.,** 'Principles of Composite Material Mechanics', McGraw-Hill, Singapore, pp. 1-33, 1994.

[2] **Fukuda, H.,** 'Stress concentration factors in unidirectional composites with random fiber spacing', Composites Science and Technology, Vol.22, pp. 153–163, 1985.

[3] **Osamura, K., Ochiai, S.,** 'Tensile strength of fiber-reinforced metal matrix composites with non-uniform fiber spacing', Journal of Materials Science , Vol. 24, pp. 3536–3540, 1989.

[4] **Osamura, K., Ochiai, S.,** 'Stress disturbance due to broken fibers in metal matrix composites with non-uniform fiber spacing', Journal of Materials Science, Vol.24, 3865–3872, 1989.

[5] **Martin A.F., Leissa A.W.,** 'Application of the Ritz method to plane elasticity problems for composite sheets with variable fiber spacing', International Journal For Numerical Methods In Engineering, Vol. 28, pp1813–1825, 1989.

[6] **Leissa A.W., Martin A.F.,** 'Vibration and buckling of rectangular composite plates with variable fiber spacing' Composite structures, Vol.14, pp339–357, 1990.

[7] **Leissa A.W., Martin A.F.,** 'Some exact plane elasticity solutions for non-homogeneous orthotropic sheets', Journal of Elasticity, Vol. 23, pp97–112, 1990.

[8] **Pandy M.D.,** 'Structure-material interaction in stability of fibrous composite elements', Ph.D. dissertation, Waterloo University, 1991.

[9] **Shiau L.C., Chue Y.H**., 'Free-edge stress reduction through fiber volume fraction variation', Composite Structures Vol.19, 145–165, 1991.

[10] **Shiau L.C., Lee G.C.,** 'Stress concentration around holes in composite laminates with variable fiber spacing', Composite Structures, Vol.24, pp 107–115, 1993.

[11] **Hutchinson, J.W.,** 'Singular Behavior at the End of a Tensile Crack in a Hardening Material', Journal of the Mechanics and Physics of Solids, vol. 16, pp. 14–31, 1968.

[12] **RICE, J.R.,** 'A Path Independent Integral and the Approximate Analysis of Strain Concentration by Notches and Cracks', Journal of Applied Mechanics - Transactions of the ASME, vol. 35, pp. 379–386, 1968.

[13] **J.K. Knowles and E. Sternberg,** 'On a Class of Conservation Laws in Linearized and Finite Elastostatics', Archive for Rational Mechanics and Analysis, vol. 44, pp. 187–211, 1972.

[14] **T.K. Hellen and W.S. Blackburn,** 'The Calculation of Stress Intensity Factors for Combined Tensile and Shear Loading', International Journal of Fracture, vol. 11, pp.605–617, 1975.

[15] **B. Budiansky and J.R. Rice,** 'Conservation Laws and Energy - Release Rates', Journal of Applied Mechanics - Transactions of the ASME, vol. 40, pp. 201–205, 1973.

[16] **W.-H. Chen and K. Ting,** 'Finite Element Analysis of Mixed – Mode Thermoelastic Fracture Problems', Nuclear Engineering and Design, vol. 90, pp. 55–65, 1985

[17] **W.-H. Chen and K. T. Chen,** 'On the Study of Mixed- mode Thermal Fracture Using Modified J_k-Integrals', International Journal of Fracture, vol. 17, pp. R99–R103, 1981.

[18] **J.H. Chang and D.J. Wu,** 'Computation of Mixed - mode Stress Intensity Factors for Curved Cracks in Anisotropic Elastic Solids', Engineering Fracture Mechanics, vol. 74, pp. 1360–1372, 2007.

[19] **S.J. Chu and C.S. Hong,** 'Application of the J_k-Integral to Mixed Mode Crack Problems for Anisotropic Composite Laminates', Engineering Fracture Mechanics, vol. 35, pp. 1093–1103, 1990.

[20] **E. Pan and B. Amadei,** 'Fracture Mechanics of Cracked 2-D Anisotropic Media with a New Formulation of the Boundary Element Method', International Journal of Fracture, vol. 77, pp. 161–174, 1996.

[21] **P. Sollero and M.H. Aliabadi,** 'Fracture Mechanics Analysis of Anisotropic Plates by the Boundary Element Method', International Journal of Fracture, vol. 64, pp. 269-284, 1993.

[22] **R. Khandelwal and J.M. Chandra Kishen,** 'Complex Variable Method of Computing J_k for Bi-Material Interface Cracks', Engineering Fracture Mechanics, vol. 73, pp. 1568–1580, 2006.

[23] **R. Khandelwal and J.M. Chandra Kishen,** 'Computation of Thermal Stress Intensity Factors for Bimaterial Interface Cracks using Domain Integral Method', Journal of Applied Mechanics-Transactions of the ASME, vol. 76, 041010, 2009.

[24] **S. Dag, E.E. Arman, and B. Yildirim,** 'Computation of Thermal Fracture Parameters for Orthotropic Functionally Graded Materials Using J_k - Integral', International Journal of Solids and Structures, vol. 47, pp. 3480–3488, 2010.

[25] **S. Dag and B. Yildirim,** 'Computation of Thermal Fracture Parameters for Inclined Cracks in Functionally Graded Materials Using J_k– Integral', Journal of Thermal Stresses, vol. 32, pp. 530–556, 2009.

[26] **S. Dag,** 'Mixed - Mode Fracture Analysis of Functionally Graded Materials Under Thermal Stresses: A New Approach Using J_k– Integral', Journal of Thermal Stresses, vol. 30, pp. 269–296, 2007.

[27] **J.W. Eischen,** 'Fracture of Nonhomogeneous Materials', International Journal of Fracture, vol. 34, pp. 3–22, 1987.

[28] **J.-H. Kim and G.H. Paulino,** 'Finite Element Evaluation of Mixed Mode Stress Intensity Factors in Functionally Graded Materials', International Journal for Numerical Methods in Engineering, vol. 53, pp. 1903–1935, 2002.

[29] **J.-H. Kim and G.H. Paulino,** 'Mixed - Mode J - Integral Formulation and Implementation Using Graded Finite Elements for Fracture Analysis of Nonhomogeneous Orthotropic Materials', Mechanics of Materials, vol. 35, pp. 107–128, 2003.

[30] **J.W. Eischen,** 'An Improved Method for Computing the J_2 Integral', Engineering Fracture Mechanics, vol. 26, pp. 691–700, 1987.

[31] **S. Dag, B. Yildirim, O. Arslan, E.E. Arman,** 'Hygrothermal Fracture Analysis of Orthotropic Materials using J_k – Integral', Journal of Thermal Stresses, vol. 35, pp-596-613, 2012.

[32] **K.Y. Lee, T.S. Lee,** 'Hygrothermal Fracture Analysis of Plastic IC Package in Reflow Soldering Process', Journal of Electronic Packaging, vol. 121, 148-156, 1999.

[33] **E. Ergun, S. Taşgetiren, M. Topçu,** 'Fatigue and Fracture Analysis of Aluminum Plate with Composite Patches under the Hygrothermal Effect', Composite Structures, vol. 92, pp-2622–263, 2010.

[34] **S. Dag and K.A. Ilhan,** 'Mixed - Mode Fracture Analysis of Orthotropic Functionally Graded Material Coatings Using Analytical and Computational methods', Journal of Applied Mechanics - Transactions of the ASME, vol. 75, 051104, 2008.

[35] **B. Yildirim, S. Yilmaz, and S. Kadioglu,** 'Delamination of Compressively Stressed Orthotropic Functionally Graded Coatings under Thermal Loading', Journal of Applied Mechanics - transactions of the ASME, vol. 75, 051106, 2008.

[36] **Dağ, S.,** 'Thermal fracture analysis of orthotropic functionally graded materials using an equivalent domain integral approach', Engineering Fracture Mechanics, Vol. 73, pp. 2802-2828, 2006.

[37] **ANSYS Inc.,** ANSYS Basic Analysis Procedures Guide, Release 5.4, Canonsburg, PA, USA, 1997.

[38] **H. S. Choi, K.J. Ahn, J.-D. Nam, H. J. Chun,** 'Hygroscopic Aspects of Epoxy/carbon Fiber Composite Laminates in Aircraft Environments', Composites: Part A: Applied science and manufacturing, Vol. 32, pp-709-720, 2001.

[39] **Shen, C. H. and Springer, G.S.,** 'Moisture absorbtion and desorption of composite materials', Journal of Composite Materials, Vol. 10, pp.2-20, 1976.

APPENDIX A

DIVERGENCE THEOREM

Divergence Theorem also known as Gauss-Ostrogradsky theorem can be stated as:

$$\int_{V} (\nabla . F) dV = \int_{\partial V} F \, da \tag{A.1}$$

Where,$V$is some region in space and ∂V is the boundary of V. Which, means a volume integral of divergence of F over V changes to a surface integral of Fover∂V.

A special case of this theorem would be considering A to be a region on the plane and Γ to be the boundary of the region and would be a line. Then:

$$\int_{A} \nabla . F \, dA = \oint_{\Gamma} F . \hat{n} \, d\Gamma \tag{A.2}$$

It can be written as:

$$\int_{A} \left(\frac{\partial F_x}{\partial x} + \frac{\partial F_y}{\partial y} \right) dx dy = \oint_{\Gamma} \left(F_x n_x + F_y n_y \right) d\Gamma \tag{A.3}$$

In indicial notation:

$$\int_{A} \left(\frac{\partial F_i}{\partial x_i} \right) dx dy = \oint_{\Gamma} (F_i n_i) d\Gamma \tag{A.4}$$

APPENDIX B

DERIVATIVES OF MECHANICAL STRAIN ENERGY DENSITY FUNCTION

In this study plane stress case is investigated, so required derivatives of mechanical strain energy density function are [36]:

$$\frac{\partial W}{\partial E_1} = -\frac{\left[\left(2E_2\nu_{12}^2 - E_1\right)\varepsilon_{11}^m + \nu_{12}E_2\varepsilon_{22}^m\right]\left[\nu_{12}E_2\varepsilon_{22}^m + E_1\varepsilon_{11}^m\right]}{2(E_1 - \nu_{12}^2E_2)^2} \tag{B.1}$$

$$\frac{\partial W}{\partial E_2} = \frac{E_1^2(\nu_{12}\varepsilon_{11}^m + \varepsilon_{22}^m)^2}{2(E_1 - \nu_{12}E_2)^2} \tag{B.2}$$

$$\frac{\partial W}{\partial \nu_{12}} = \frac{E_1E_2(\nu_{12}\varepsilon_{11}^m + \varepsilon_{22}^m)(\nu_{12}E_2\varepsilon_{22}^m + E_1\varepsilon_{11}^m)}{(E_1 - \nu_{12}^2E_2)^2} \tag{B.3}$$

$$\frac{\partial W}{\partial G_{12}} = \varepsilon_{12}^2 + \varepsilon_{21}^2 \tag{B.4}$$

$$\frac{\partial W}{\partial \alpha_1} = -\frac{E_1(\nu_{12}E_2\varepsilon_{22}^m + E_1\varepsilon_{11}^m)\Delta T}{E_1 - \nu_{12}^2E_2} \tag{B.5}$$

$$\frac{\partial W}{\partial \alpha_2} = -\frac{E_1E_2(\nu_{12}\varepsilon_{11}^m + \varepsilon_{22}^m)\Delta T}{E_1 - \nu_{12}^2E_2} \tag{B.6}$$

$$\frac{\partial W}{\partial \Delta T} = -\frac{E_1[(E_1\alpha_1 + \nu_{12}E_2\alpha_2)\varepsilon_{11}^m + (E_2\alpha_2 + \nu_{12}E_2\alpha_1)\varepsilon_{22}^m]}{E_1 - \nu_{12}^2E_2} \tag{B.7}$$

$$\frac{\partial W}{\partial \beta_1} = -\frac{E_1(\nu_{12}E_2\varepsilon_{22}^m + E_1\varepsilon_{11}^m)\Delta c}{E_1 - \nu_{12}^2E_2} \tag{B.8}$$

$$\frac{\partial W}{\partial \beta_2} = -\frac{E_1E_2(\nu_{12}\varepsilon_{11}^m + \varepsilon_{22}^m)\Delta c}{E_1 - \nu_{12}^2E_2} \tag{B.9}$$

$$\frac{\partial W}{\partial \Delta c} = -\frac{E_1[(E_1\beta_1 + \nu_{12}E_2\beta_2)\varepsilon_{11}^m + (E_2\beta_2 + \nu_{12}E_2\beta_1)\varepsilon_{22}^m]}{E_1 - \nu_{12}^2E_2} \tag{B.10}$$

APPENDIX C

DEVELOPED ANSYS APDL CODE

Material properties input written in the APDL code for ANSYS:

```
NUMCMP,ELEMENT
NMAT=0
CSYS,0
WPCSYS,-1,0
CSYS,0
WPAVE,0,0,0

MPTEMP,0, TZEROT

*GET,N1EL,ELEM,0,NUM,MIND
*GET,N2EL,ELEM,0,NUM,MAXD

*DO,IKP,N1EL,N2EL
!GET THE CENTROIDAL COORDINATES OF EACH ELEMENT
*GET,XCEL,ELEM,IKP,CENT,X
*GET,YCEL,ELEM,IKP,CENT,Y

NMAT=NMAT+1

VOLF=Vf0+(Vfw-Vf0)*(YCEL/h)**P
VOLMA=1-VOLF

! Hygroscopic props

E1M=EF*VOLF+EMA*VOLMA                          ! young modulus
E2M=EMA*EF/(EMA*VOLF+VOLMA*EF)                 ! young modulus
V12M=VF*VOLF+VMA*VOLMA                         ! poisson ratio
G12M=G12MA*G12F/(VOLF*G12MA+G12F*VOLMA)        ! Rigidity
ROM=ROF*VOLF+ROMA*VOLMA                        ! density
B1M=EMA*ROM*BMA/(E1M*ROMA)                     ! swelling coefficient sat conc.
B2M=(1+VMA)*ROM*BMA/ROMA                       ! swelling coefficient  sat conc.
D1M=(1-VOLF)*DIFMA                             ! diffusion constant
D2M=(1-2*SQRT(VOLF/pi))*DIFMA                  ! diffusion constant

! Thermal props

E1TR=E1M                                       !! young modulus
E2TR=E2M                                       !! young modulus
V12TR=V12M                                     !! poisson ratio
G12TR=G12M                                     !! Rigidity
ROTR=ROM                                       !! density
A1TR=(ALF*EF*VOLF+ALMA*EMA*VOLMA)/E1TR         !! Thermal expansion. coefficient.
A2TR=(1+VF)*ALF*VOLF+(1+VMA)*ALMA*VOLMA-A1TR*V12TR
CTR1=VOLF*CNF+VOLMA*CNM
MUTR=((CNF/CNM)-1)/((CNF/CNM)+1)
```

```
CTR2=(1+MUTR*VOLF)*CNM/(1-MUTR*VOLF)

MPDATA,EX,NMAT,,E1TR
MPDATA,EY,NMAT,,E2TR
MPDATA,PRXY,NMAT,,V12TR
MPDATA,GXY,NMAT,,G12TR
MPDATA,ALPX,NMAT,,A1TR
MPDATA,ALPY,NMAT,,A2TR
MPDATA,KXX,NMAT,,CTR1
MPDATA,KYY,NMAT,,CTR2

MPCHG,NMAT,IKP,
*ENDDO
```

Main part of the code containing shape functions written for calculation of integral using Gauss Quadrature:

```
*DO,IGAUS,1,2,1

I=IGAUS
J=I

SHAPE(1)=-0.25*(1-S(I))*(1-T(J))*(1+S(I)+T(J))
SHAPE(2)=-0.25*(1+S(I))*(1-T(J))*(1-S(I)+T(J))
SHAPE(3)=-0.25*(1+S(I))*(1+T(J))*(1-S(I)-T(J))
SHAPE(4)=-0.25*(1-S(I))*(1+T(J))*(1+S(I)-T(J))
SHAPE(5)=0.5*(1-S(I)**2)*(1-T(J))
SHAPE(6)=0.5*(1-T(J)**2)*(1+S(I))
SHAPE(7)=0.5*(1-S(I)**2)*(1+T(J))
SHAPE(8)=0.5*(1-T(J)**2)*(1-S(I))

SHAPEDS(1)=0.25*(1-T(J))*(2*S(I)+T(J))
SHAPEDS(2)=0.25*(1-T(J))*(2*S(I)-T(J))
SHAPEDS(3)=0.25*(1+T(J))*(2*S(I)+T(J))
SHAPEDS(4)=0.25*(1+T(J))*(2*S(I)-T(J))
SHAPEDS(5)=-S(I)*(1-T(J))
SHAPEDS(6)=0.5*(1-T(J)**2)
SHAPEDS(7)=-S(I)*(1+T(J))
SHAPEDS(8)=-0.5*(1-T(J)**2)

SHAPEDT(1)=0.25*(1-S(I))*(2*T(J)+S(I))
SHAPEDT(2)=0.25*(1+S(I))*(2*T(J)-S(I))
SHAPEDT(3)=0.25*(1+S(I))*(2*T(J)+S(I))
SHAPEDT(4)=0.25*(1-S(I))*(2*T(J)-S(I))
SHAPEDT(5)=-0.5*(1-S(I)**2)
SHAPEDT(6)=-T(J)*(1+S(I))
SHAPEDT(7)=0.5*(1-S(I)**2)
SHAPEDT(8)=-T(J)*(1-S(I))

SL1=0.5*(2*LS(I)-1)
SL2=0.5*(2*LS(I)+1)
SL3=-LS(I)*2.

YGAUS0=0.
XGAUS0=0.
YGAUS=0.
XGAUS=0.
```

```
TEMPGAUS=0.
SUM1=0.
SUM2=0.
SUM3=0.
SUM4=0.


*DO,IN,1,8,1
SUM1=SUM1+SHAPEDS(IN)*LOCX_(IN)
SUM2=SUM2+SHAPEDT(IN)*LOCY_(IN)
SUM3=SUM3+SHAPEDT(IN)*LOCX_(IN)
SUM4=SUM4+SHAPEDS(IN)*LOCY_(IN)
YGAUS0=YGAUS0+SHAPE(IN)*LOCY0_(IN)
XGAUS0=XGAUS0+SHAPE(IN)*LOCX0_(IN)
XGAUS=XGAUS+SHAPE(IN)*LOCX_(IN)
YGAUS=YGAUS+SHAPE(IN)*LOCY_(IN)
TEMPGAUS=TEMPGAUS+SHAPE(IN)*TEMP_(IN)
*ENDDO

DETLINE=abs(SL1*C1+SL2*C2+SL3*C3)
DET=SUM1*SUM2-SUM3*SUM4

*IF,ste,EQ,1,THEN

VOLFGAUS=Vf0+(Vfw-Vf0)*(YGAUS0/h)**P
VOLMAGAUS=1-VOLFGAUS
E1GAUS=EF*VOLFGAUS+EMA*VOLMAGAUS
E2GAUS=EMA*EF/(EMA*VOLFGAUS+VOLMAGAUS*EF)
V12GAUS=VF*VOLFGAUS+VMA*VOLMAGAUS
G12GAUS=G12MA*G12F/(VOLFGAUS*G12MA+G12F*VOLMAGAUS)
AL1GAUS=(ALF*EF*VOLFGAUS+ALMA*EMA*VOLMAGAUS)/E1GAUS
AL2GAUS=(1+VF)*ALF*VOLFGAUS+(1+VMA)*ALMA*VOLMAGAUS-
AL1GAUS*V12GAUS
TETGAUS=TEMPGAUS-TZEROP

*ELSE

VOLFGAUS=Vf0+(Vfw-Vf0)*(YGAUS0/h)**P
VOLMAGAUS=1-VOLFGAUS
E1GAUS=EF*VOLFGAUS+EMA*VOLMAGAUS
E2GAUS=EMA*EF/(EMA*VOLFGAUS+VOLMAGAUS*EF)
V12GAUS=VF*VOLFGAUS+VMA*VOLMAGAUS
G12GAUS=G12MA*G12F/(VOLFGAUS*G12MA+G12F*VOLMAGAUS)
 ROMGAUS=ROF*VOLFGAUS+ROMA*VOLMAGAUS
AL1GAUS=EMA*ROMGAUS*BMA/(E1GAUS*ROMA)
AL2GAUS=(1+VMA)*ROMGAUS*BMA/ROMA
TETGAUS=TEMPGAUS-TZEROP
*ENDIF

*DO,IN,1,8,1
DNDA=SHAPEDS(IN)/DET
DNDB=SHAPEDT(IN)/DET
DNDX(IN)=DNDA*SUM2-DNDB*SUM4
DNDY(IN)=SUM1*DNDB-SUM3*DNDA
*ENDDO


*DO,IN,1,4,1
```

```
LSN(IN)=0.
*ENDDO

*DO,IN,1,8,1
LSN(1)=LSN(1)+DNDX(IN)*DISPX_(IN)
LSN(2)=LSN(2)+DNDY(IN)*DISPY_(IN)
LSN(3)=LSN(3)+(DNDX(IN)*DISPY_(IN)+DNDY(IN)*DISPX_(IN))/2
*ENDDO


WI1=LSN(1)-AL1GAUS*TETGAUS
WI2=LSN(2)-AL2GAUS*TETGAUS
WI3=E1GAUS-(V12GAUS**2)*E2GAUS
WE1=((E1GAUS**2)*WI1+V12GAUS*E1GAUS*E2GAUS*WI2)*WI1/(2*WI3)
WE2=G12GAUS*2*(SN(3)**2)
WE3=(V12GAUS*E1GAUS*E2GAUS*WI1+E1GAUS*E2GAUS*WI2)*WI2/(2*WI3)

LWORK=WE1+WE2+WE3
INTEG=INTEG+LWORK*((R-ABS(XGAUS))/R)*DETLINE

*ENDDO
```